NASA Technical Memorandum 83671

A Theoretical Model for the Cross Spectra Between Pressure and Temperature Downstream of a Combustor

J. H. Miles and E. A. Krejsa
Lewis Research Center
Cleveland, Ohio

Prepared for the
One hundred seventh Meeting of the Acoustical Society of America
Norfolk, Virginia, May 6–10, 1984

NASA

A THEORETICAL MODEL FOR THE CROSS SPECTRA BETWEEN PRESSURE AND TEMPERATURE DOWNSTREAM OF A COMBUSTOR

J. H. Miles and E. A. Krejsa
National Aeronautics and Space Administration
Lewis Research Center
Cleveland, Ohio 44135

SUMMARY

A theoretical model developed to calculate pressure-temperature cross spectra, pressure spectra, temperature spectra and pressure cross spectra in a ducted combustion system is presented. The model assumes the presence of a fluctuating-volumetric-heat-release-rate disk source and takes into account the spatial distribution of the steady-state volumetric-heat flux. Using the model, pressure, velocity, and temperature perturbation relationships can be obtained. The theoretical results show that, at a given air mass flow rate, the calculated pressure-temperature cross spectra phase angle at the combustor exit depends on the model selected for the steady-state volumetric-heat flux in the combustor. Using measurements of the phase angle, an appropriate source region model was selected. The model calculations are compared with the data. The comparison shows good agreement and indicates that with the use of this model the pressure-temperature cross spectra measurements provide useful information on the physical mechanisms active at the combustion noise source.

E-2114

NOMENCLATURE

$\mathscr{A}$	see Eq. (46)
A	area, m^2
B	see Eq. (30)
C	see Eq. (47)
D	see Eq. (45)
c_o	sound propagation speed, m/s
c_p	gas specific heat at constant pressure, J/kg-K
c_v	gas specific heat at constant volume, J/kg-K
d	diameter,m
f	frequency, Hz
G	see Eq. (25)
H	see Eq. (24)
i	$(-1)^{1/2}$
J	see Eq. (54)
j	summation index
K	see Eq. (26)
K'	see Eq. (26)

k	ω/c_0
$\mathscr{L}$	see Eq. (27)
L	distance between points
ℓ	summation index
$\mathscr{M}$	see Eq. (28)
M	Mach number
(MW)	gas molecular wt.
N	number of regions
P	see Eq. (45)
p	acoustic pressure, Pa
Q_0, Q_1	volumetric-heat-release-rate coefficients
q	volumetric-heat-release rate
$\mathscr{R}$	gas constant
R	pressure reflection coefficient
r	nozzle exit radius
$\mathscr{S}$	see Eq. (54)
s	gas entropy, J/kg-K
T	transfer matrix
t	temperature, K
u	mean flow gas velocity
W	mass flow rate, kg/s
x	cartesian coordinate
Y	see Eq. (29)
Z	acoustic impedance
γ	specific heat ratio of gas
δ	unit impulse function
ε	see Eq. (56)
ξ	see Eq. (62)
η	see Eq. (65)
θ	time, s
$\lambda_1, \lambda_2, \lambda_3$	see Eq. (51)
ν	see Eq. (55)
ρ	gas density, kg/m
σ	see Eq. (65)
ω	angular frequency, $2\pi f$

Superscripts:

*	complex conjugate
T	transpose
( )	instantaneous quantity

Subscripts:

$( )_0$	reference quantity
$( )_1$	perturbed quantity
$( )_{CIN}$	combustor inlet
$( )_{EXIT}$	duct exit
$( )_g$	gas
$( )_{INLET}$	duct inlet
$( )_S$	source

INTRODUCTION

Combustion noise occurs in many systems (refs. 1 and 2) and is an important noise source in turbine-powered aircraft and helicopters (refs. 3 and 4). The NASA Lewis Research Center turbine engine core noise research program involved tests in turbine engines, engine component facilities, and small scale rigs using in-house, contractor, and university facilities. As part of this research program, various measurement techniques were developed to study noise associated with combustion rigs and aircraft engines. The experimental techniques using unsteady pressure measurements to study core noise included: coherence measurements (refs. 5 and 6), conditional spectral analysis (ref. 6), modal analysis (refs. 7 and 8), three signal coherence analysis (refs. 9 to 11), cepstral analysis (ref. 12) and pressure-temperature cross spectra (refs. 13 and 14). Note that the last technique also includes temperarture measurements.

In analyzing combustion noise measurements two common assumptions are made: the same basic source mechanism is present for all tests, and the magnitude of the noise depends on a single parameter, related to the heat-release rate, that can be calculated from the steady state operating conditions and the geometry. Thus, the existence of a relationship between the combustion noise and the combustion process has generally been established by determining that a correlation between the combustion noise and a steady-state heat-release rate parameter exists (refs. 10, 12, and 15 to 17) rather than by any direct physical measurement of a fluctuating quantity. The parameter used to correlate combustion noise can be selected using a theoretical model (ref. 17) or judicious curve fitting (refs. 10 and 16). In either case, the effectiveness is decided by examining the ability of the parameter to correlate noise measurements at many test conditions.

Unfortunately, this approach does not yield any information about possible physical mechanisms active at the combustion source. Note that this is in strong distinction to the case of flow noise due to a solid body in contact with airflow containing velocity and pressure fluctuations. In this case, the various physical mechanisms are known and the assumption is made that predicting flow noise requires the specification of air stream mean velocity, rms

turbulence intensity, correlation lengths, and turbulence spectra (ref. 18). However, most of these quantities can not be determined from the mean operating conditions and test geometry but have to be measured at each test condition.

The importance of a physical mechanism is tested by including it in a theoretical model which is used to calculate results that can be compared with measurements. Analytical one-dimensional models for combustion noise generation and propagation in constant and variable area ducts were developed both at NASA Lewis and with NASA Lewis support (refs. 19 to 28) to compare with experimental measurements. Even though these models yield acoustic pressure spectra, cross spectra and transfer functions that resemble measured data this agreement is not sufficient to determine which source region model is appropriate since similar acoustic results are obtained for different source region models.

Measurements were made of pressure-temperature cross spectra (refs. 13 to 14) along with pressure auto spectra and cross spectra to select an appropriate source model and to provide information on the physical mechanisms in the combustion noise source region. The simultaneous real-time measurement of temperature and pressure fluctuations in a duct is not new or unique and neither is the derivation of auto spectra from them (refs. 29 to 32). However, the use of the cross spectra between pressure and temperature to show that a physical connection between the heat-release rate and the combustion noise does exist is new and unique (refs. 13 and 14) as is the use of this data to develop a model.

In the next section, the model developed to analyze measurements of pressure-temperature cross spectra, pressure spectra, temperature spectra and pressure cross spectra made in a combustion duct is presented. Then the experimental investigation is discussed and the model results are compared with experimental measurements.

ANALYTICAL MODEL

A theoretical model developed to calculate pressure-temperature cross spectra, pressure spectra, temperature spectra and pressure cross spectra in a ducted combustion system is presented. The model assumes the presence of a fluctuating-volumetric-heat-release-rate disk source and takes into account the spatial distribution of the steady-state volumetric-heat flux. A solution is obtained by solving an inhomogeneous differential equation using three boundary equations. One boundary condition is obtained by assuming the inlet gas behaves adiabatically. A second is based on using a pressure reflection coefficient at the combustor entrance. The third is due to assuming a flanged pipe pressure boundary condition at the exit. Using the model, pressure, velocity, and temperature perturbation relationships can be obtained. The model equations used are similar to those discussed in references 20 and 21. The model developed to calculate pressure-temperature cross spectra includes terms dependent on a space-dependent-volumetric-heat-source region in addition to terms dependent on area gradients. While, the experimental data were obtained in a constant area combustion rig, the equations presented are for the more general case. In references 20 and 21, these equations were used only to calculate pressure spectra. In this paper,they are used to generate temperature spectra and pressure-temperature cross spectra. The equations are solved using a transfer matrix approach rather than by direct numerical integration

as in references 20 and 21. This method gives perhaps more physical insight at the expense of some additional analytical work. However, including a distributed volumetric heat-release rate perturbation source region is also more difficult. Consequently, the calculations are for a single disk source volumetric-heat-flux-rate perturbation. Models have been developed previously for sound propagation in a duct with an axial temperature gradient (refs. 33 to 39), however, they do not include a heat source.

Governing Equations

The one dimensional continuity, momentum, and energy equations for the bulk gas are:

$$A\left[\frac{\partial \hat{\rho}}{\partial \theta} + \hat{u}\frac{\partial \hat{\rho}}{\partial x}\right] + A\hat{\rho}\frac{\partial \hat{u}}{\partial x} + \hat{\rho}\hat{u}\frac{\partial A}{\partial x} = 0 \tag{1}$$

$$\hat{\rho}\left[\frac{\partial \hat{u}}{\partial \theta} + \hat{u}\frac{\partial \hat{u}}{\partial x}\right] = -\frac{\partial \hat{p}}{\partial x} \tag{2}$$

$$\hat{\rho}\hat{t}\left[\frac{\partial}{\partial \theta} + \hat{u}\frac{\partial}{\partial x}\right]\hat{s} = \hat{q} \tag{3}$$

where $\hat{p}$, $\hat{\rho}$, $\hat{u}$, $\hat{t}$, $\hat{s}$, and $\hat{q}$ are respectively the instantaneous pressure, density, velocity, temperature, entropy and volumetric-heat-release rate. The bulk gas is characterized by two equations:

$$\hat{p} = \frac{\hat{\rho}\mathcal{R}\hat{t}}{(MW)} \tag{4}$$

$$\hat{s} = s_o + c_v \ln\left(\hat{p}/\hat{\rho}^{\gamma}\right) \tag{5}$$

where

$$c_p - c_v = \mathcal{R}/(MW)$$

and

$$\gamma = c_p/c_v$$

Equations (1) to (5) are linearized by assuming each of the variables $\hat{p}$, $\hat{\rho}$, $\hat{u}$, $\hat{t}$, $\hat{s}$, and $\hat{q}$ consists of a steady component that is a function of axial position designated by the subscript $(\ )_0$ and a small perturbation that is a function of axial position and time designated by $(\ )_1$. The steady components are assumed to change gradually. Consequently, in small regions they can be considered to be constant. The steady state components satisfy the following zeroth-order system of equations:

$$\frac{1}{p_o}\frac{dp_o}{dx} - \frac{1}{t_o}\frac{dt_o}{dx} + \frac{1}{u_o}\frac{du_o}{dx} + \frac{1}{A}\frac{dA}{dx} = 0 \tag{8}$$

$$\rho_o u_o \frac{du_o}{dx} + \frac{dp_o}{dx} = 0 \tag{9}$$

$$\frac{1 - \gamma}{\gamma} \frac{dp_o}{dx} + \frac{p_o}{t_o} \frac{dt_o}{dx} = \left(\frac{\gamma - 1}{\gamma}\right) \frac{q_o}{u_o} \tag{10}$$

The solution to equations (8) to (10) was obtained by direct integration with the Runge-Kutta method (ref. 40) after rewriting the system of equations as follows:

$$\frac{d \ln p_o}{dx} = \left(\frac{M_o^2}{M_o^2 - 1}\right) \left[- \frac{\gamma d \ln A}{dx} + \frac{(\gamma - 1)}{p_o u_o} q_o\right] \tag{11}$$

$$\frac{d \ln u_o}{dx} = \frac{1}{M_o^2 - 1} \left[\frac{d \ln A}{dx} - \frac{(\gamma - 1)}{\rho_o c_o^2} \frac{q_o}{u_o}\right] \tag{12}$$

$$\frac{d \ln t_o}{dx} = \frac{M_o^2}{M_o^2 - 1} \left[(1 - \gamma) \frac{d \ln A}{dx} + \frac{(\gamma - 1)(M_o^2 \gamma - 1)}{\rho_o u_o^2 u_o} q_o\right] \tag{13}$$

where

$$c_o^2 = \frac{\gamma \mathcal{R} t_o}{(MW)} = \gamma p_o / \rho_o \tag{14}$$

and

$$M = u_o / c_o \tag{15}$$

In performing the integration the steady state inlet boundary conditions are selected to match the measured inlet mass flow, pressure and temperature conditions and a volumetric-heat-source distribution is selected so that the calculated temperatures in the long duct are similar to the measured temperatures.

The perturbed components satisfy the following first-order system of equations:

$$\frac{1}{u_o} \frac{\partial}{\partial \theta} \left(\frac{p_1}{p_o} - \frac{t_1}{t_o}\right) + \left(\frac{d \ln \rho_o}{dx} + \frac{d \ln A}{dx}\right) \frac{u_1}{u_o} + \left(\frac{d \ln u_o}{dx} + \frac{d \ln A}{dx}\right) \left(\frac{p_1}{p_o} - \frac{t_1}{t_o}\right) + \left(\frac{1}{p_o} \frac{\partial p_1}{\partial x} - \frac{1}{t_o} \frac{\partial t_1}{\partial x}\right) + \frac{1}{u_o} \frac{\partial u_1}{\partial x} = 0 \tag{16}$$

$$\rho_o \left(\frac{\partial}{\partial \theta} + u_o \frac{\partial}{\partial x}\right) u_1 + \rho_o u_o \left(\frac{du_o}{dx}\right) \left(\frac{p_1}{p_o} - \frac{t_1}{t_o}\right) + \partial p_1 / \partial x + \rho_o u_1 du_o / dx = 0 \tag{17}$$

$$p_o \left[\frac{\partial}{\partial\theta} + u_o \frac{\partial}{\partial x}\right] \left[-\frac{p_1}{p_0} + \left(\frac{\gamma}{\gamma - 1}\right) \frac{t_1}{t_0}\right] + \frac{p_1}{p_0} q_0 + \frac{u_1}{u_0} q_0 = q_1 \tag{18}$$

In order to solve equations (16) to (18) the periodic solutions are assumed to have the form:

$$p_1(\theta,x) = p_1(x)\ e^{-i\omega\theta} \tag{19}$$

$$\mu_1(\theta,x) = u_1(x)\ e^{-i\omega\theta} \tag{20}$$

$$t_1(\theta,x) = t_1(x)\ e^{-i\omega\theta} \tag{21}$$

$$q_1(\theta,x) = q_1\ e^{-i\omega\theta}\ \delta(x - x_s) \tag{22}$$

Note that the fluctuating volumetric-heat-flux rate is assumed to be a constant independent of frequency and to be located on a disk at x_s. Substituting equations (19) to (22) into equations (16) to (18) yields the following equation in matrix form for the spatial distribution of the perturbed quantities:

$$H \frac{dY}{dx} + GY = K \tag{23}$$

where

$$H = \begin{bmatrix} 1/p_o & 1/u_o & -1/t_o \\ 1/\rho_o & u_o & 0 \\ -(\gamma - 1)/\gamma & 0 & p_o/t_o \end{bmatrix} \tag{24}$$

$$G = \begin{bmatrix} -\left(\frac{i\omega}{u_o} + \mathscr{L}\right)/p_o & \frac{\mathscr{M}}{u_o} & -\left(-\frac{i\omega}{u_o} + \mathscr{L}\right)/t_o \\ \frac{u_o^2}{p_o} \frac{d\ln u_o}{dx} & \left(-i\omega + \frac{du_o}{dx}\right) & -\frac{u_o^2}{t_o} \frac{d\ln u_o}{dx} \\ \left(\frac{i\omega}{u_o} + \frac{q_o}{u_o p_o}\right)\left(\frac{\gamma - 1}{\gamma}\right) & \frac{q_o}{u_o^2}\left(\frac{\gamma - 1}{\gamma}\right) & \left(-\frac{i\omega}{u_o}\right)\frac{p_o}{t_o} \end{bmatrix} \tag{25}$$

$$K = \left[\frac{q_1}{q_0}\left(\frac{\gamma - 1}{\gamma}\right) \delta(x - x_s)\right] = K'\delta(x - x_s) \tag{26}$$

$$\mathscr{L} = \frac{d \ln u_o}{dx} + \frac{d \ln A}{dx} \tag{27}$$

$$\mathcal{M} = \frac{d \ln \rho_0}{dx} + \frac{d \ln A}{dx} \tag{28}$$

and

$$Y = (p_1, u_1, t_1)^T \tag{29}$$

where T is the transpose.

Nonsource Region

In the region where the unsteady heat release rate is zero, the resulting homogeneous differential equation is

$$\frac{dY}{\partial x} = H^{-1} GY = BY \tag{30}$$

where

$$B_{11} = \frac{M_0^2}{1 - M_0^2} \left[\left(-\frac{i\omega}{u_0} \right) + \frac{\gamma d \ln A}{dx} + \frac{(\gamma - 1)}{u_0 p_0} q_0 \right] \tag{31}$$

$$B_{12} = \frac{\rho_0 c_0}{1 - M_0^2} \left[\left(\frac{i\omega}{c_0} \right) + \frac{2M_0}{1 - M_0^2} \frac{d \ln H}{dx} - \frac{q_0}{p_0} \frac{1}{1 - {}_0M^2} \left(\frac{\gamma - 1}{\gamma} \right) \left\{ \frac{2M}{u_0} + \frac{(M_0^2 - 1)}{c_0} \right\} \right] \tag{32}$$

$$B_{13} = - \frac{M_0^2}{(1 - M_0^2)} \frac{p_0}{t_0} \frac{\gamma d \ln A}{dx} \tag{33}$$

$$B_{21} = \frac{1}{(1 - M_0^2) \rho_0 c_0} \left[\frac{i\omega}{c_0} - 2 \left(\frac{q_0}{c_0} \right) \frac{(\gamma - 1)}{p_0} \right] \tag{34}$$

$$B_{22} = \frac{M_0}{1 - M_0^2} \left(- \frac{i\omega}{c_0} \right) - \frac{(M_0^2 + 1)}{\left(1 - M_0^2\right)^2} \frac{d \ln A}{dx} - \frac{q_0}{p_0} \frac{(\gamma - 1)}{\gamma u_0} \left[1 + \left(\frac{M_0^2 + 1}{M_0^2 - 1} \right) \right] \frac{1}{(1 - M_0^2)} \tag{35}$$

$$B_{23} = \left(\frac{1}{t_0} \right) \frac{1}{1 - M_0^2} \frac{(\gamma - 1)}{\rho c_0^2} q_0 \tag{36}$$

$$B_{31} = -\frac{1}{(1 - M_o^2)} \frac{t_o}{p_o} \left[\left(-\frac{i\omega}{u_o} \right) \left(\frac{\gamma - 1}{\gamma} \right) - M_o^2 (1 - \gamma) \frac{d \ln A}{dx} \right.$$

$$\left. + (\gamma M_o^2 - 1) \frac{q_o}{p_o u_o} \left(\frac{\gamma - 1}{\gamma} \right) \right] \tag{37}$$

$$B_{32} = \frac{t_o}{(1 - M_o^2)} \left(-(1 - \gamma) M_o \left(\frac{i\omega}{c_o} \right) + 2 \left(\frac{1 - \gamma}{\gamma} \right) \frac{M_o^2}{(M_o^2 - 1)} \frac{d \ln A}{dx} \right.$$

$$\left. + \frac{q_o(\gamma - 1)}{u_o p_o \gamma} \left[\left(\gamma M_o^2 - 1 \right) - \frac{(1 - \gamma) 2M_o^2}{M_o^2 - 1} \right] \right) \tag{38}$$

$$B_{33} = \frac{i\omega}{u_o} + \frac{M_o^2}{(1 - M_o^2)} (1 - \gamma) \frac{d \ln A}{dx} \tag{39}$$

For the general case, an approximate solution to equation (30) can be obtained in terms of a transmission matrix by dividing the nonsource region into a number of regions or subsections where steady-state quantities such as the Mach number and heat-release rate in each region can be assumed constant and the area variation in each region can be approximated by an exponential area variation. Note that in applying these equations to the particular test configuration used the area is constant and the area variation is zero.

With these assumptions the B matrix is independent of x in the evaluation region. Thus the solution to equation (30) for the j^{th} region is

$$Y(x_j + \Delta x_j) = \left(e^{B_j \Delta x_j} \right) Y(x_j) \tag{40}$$

where Δx is the length of the j^{th} region and $\exp(B_j \Delta x_j)$ is the matrix exponential. The matrix $\exp(B_j \Delta x_j)$ is the transmission matrix of the j^{th} region $(T)_j$ so that

$$(T)_j = e^{B_j \Delta x_j} = \sum_{\ell=0}^{\infty} \frac{(B_j \Delta x_j)^\ell}{\ell!} = \begin{bmatrix} T_{11} & T_{12} & T_{13} \\ T_{21} & T_{22} & T_{23} \\ T_{31} & T_{32} & T_{33} \end{bmatrix} \tag{41}$$

Consequently, in a region without sources the transmission matrix is found from

$$Y(x = L) = \prod_{J=1}^{N} e^{(B_j \Delta x_j)} \; Y(x = 0) = T\, Y(x = 0) \tag{42}$$

where

$$L = \sum_{j=1}^{N} (\Delta x)_j \tag{43}$$

and N is the number of regions. While the series given in equation (42) defines the matrix exponential, it was not used for computer calculation since the convergence of the series may be slow. The matrix exponential was evaluated from

$$e^{B\Delta x} = C^{-1}\, P\, e^{D\Delta x}\, P^{-1} C \tag{44}$$

where

$$D = P^{-1} \mathscr{A} P \tag{45}$$

$$\mathscr{A} = C\, B\, C^{-1} \tag{46}$$

$$C = \begin{bmatrix} 1 & 0 & 0 \\ 0 & \rho_o c_o & 0 \\ 0 & 0 & p_o/t_o \end{bmatrix} \tag{47}$$

and P is determined to make the D matrix is diagonal. The P matrix consists of the eigenvectors of $\mathscr{A}$.

The P matrix used has the following elements for j = 1,2, and 3

$$P(1,j) = (\mathscr{A}_{33} - \lambda_j)(\mathscr{A}_{22} - \lambda_j) - \mathscr{A}_{32}\mathscr{A}_{23} \tag{48}$$

$$P(2,j) = -\left[(\mathscr{A}_{21}\mathscr{A}_{33} - \lambda_j) - \mathscr{A}_{31}\mathscr{A}_{23}\right] \tag{49}$$

$$P(3,j) = \mathscr{A}_{21}\mathscr{A}_{32} - \mathscr{A}_{31}(\mathscr{A}_{22} - \lambda_j) \tag{50}$$

The values of λ_1, λ_2, and λ_3 are the eigenvalues of the matrix. These values are the roots of

$$\begin{aligned} &(\mathscr{A}_{33} - \lambda)\left[(\mathscr{A}_{11} - \lambda)(\mathscr{A}_{22} - \lambda) - \mathscr{A}_{21}\mathscr{A}_{12}\right] \\ &+\mathscr{A}_{23}\left[\mathscr{A}_{12}\mathscr{A}_{31} - (\mathscr{A}_{11} - \lambda)(\mathscr{A}_{32})\right] \\ &+\mathscr{A}_{13}\left[\mathscr{A}_{31}\mathscr{A}_{32} - \mathscr{A}_{31}(\mathscr{A}_{22} - \lambda)\right] = 0 \end{aligned} \tag{51}$$

It can be verified that

$$D = \begin{pmatrix} \lambda_1 & 0 & 0 \\ 0 & \lambda_2 & 0 \\ 0 & 0 & \lambda_3 \end{pmatrix} \tag{52}$$

hence

$$e^{D\Delta x} = \begin{pmatrix} e^{\lambda_1 \Delta x} & 0 & 0 \\ 0 & e^{\lambda_2 \Delta x} & 0 \\ 0 & 0 & e^{\lambda_3 \Delta x} \end{pmatrix} \tag{53}$$

Nozzle Boundary Condition

The duct exit impedance used is

$$\frac{p(i\omega)}{\rho_0 c_0 u(i\omega)} = \frac{Z}{\rho_0 c_0}\bigg|_{EXIT} = 1 - \frac{2J_1(v)}{v} - \frac{2i\mathcal{S}(v)}{v} \tag{54}$$

where

$$v = 2\,k\,r \tag{55}$$

$J_1(v)$ is the Bessel function of the first order and first kind, $S(v)$ is the Struve function of the first order and first kind and r is the nozzle exit radius. This is the impedance of a circular duct with no flange having an open end fitted with an infinite acoustically rigid flange (ref. 41).

Source Region

The source region solution is obtained by integrating equation (23) over a small interval, ε.

$$\int_{x-\varepsilon}^{x+\varepsilon} \left(\frac{HdY}{dx}\right) dx + \int_{x-\varepsilon}^{x+\varepsilon} GY dx = \int_{x-\varepsilon}^{x+\varepsilon} K'\delta(x - x_s)\, dx \tag{56}$$

and letting ε go to zero. Since Y is continuous, the second integral will tend to zero as ε, and thus the first quantity must have the finite value K'. Thus

$$H(Y_{x+\varepsilon} - Y_{x-\varepsilon}) = K' \tag{57}$$

Furthermore,

$$Y_{x+\varepsilon} = T_{EXIT}\, Y_{EXIT} \tag{58}$$

$$Y_{x-\varepsilon} = T_{CIN}\, Y_{CIN} \tag{59}$$

where

$$Y_{EXIT} = \begin{pmatrix} 1 \\ 1/Z_{EXIT} \\ \xi_{EXIT} \end{pmatrix} P_{EXIT} \tag{60}$$

$$Y_{CIN} = \begin{pmatrix} 1 \\ 1/Z_{CIN} \\ \xi_{CIN} \end{pmatrix} P_{CIN} \tag{61}$$

$$\xi = t(i\omega)/p(i\omega) \tag{62}$$

At the combustor inlet the impedance is written in terms of a reflection coefficient:

$$\frac{Z_{CIN}}{\rho_o c_o} = \frac{1 + R_{CIN}}{1 - R_{CIN}} \tag{63}$$

Also at the inlet the gas is assumed to behave adiabatically

$$\xi_{CIN} = \left(\frac{t_o}{p_o}\right) \frac{\gamma - 1}{\gamma} = \left.\frac{t(i\omega)}{p(i\omega)}\right|_{CIN} \tag{64}$$

The resulting linear system of equations consists of three equations and has three unknowns. The unknown quantities are the pressure perturbations at the combustor inlet and the duct exit and the pressure-temperature perturbation relationship at the duct exit. Consequently, for a given heat-release-rate perturbation the quantities can be determined as a function of frequency.

EXPERIMENTAL INVESTIGATION

The temperature and pressure measurements were made in the combustion rig shown in figure 1, which consisted of a J-47 can combustor (fig. 1(b)) mounted in a 0.203-m-diameter by 0.77-m-long test section and an attached 6.44-m-long by 0.203-m-diameter stainless-steel duct. The fuel used was hydrogen. Pressure and temperature measurements at stations 3 and 4 are discussed. All tests were conducted at the outdoor acoustic arena shown in figure 2. Tests were run for a range of conditions. Presented are measurements made at two of the test conditions shown in table I. Note that for the higher air mass flow rate cases the long duct exit temperature is greater than the inlet temperature indicating some burning is occurring in the long duct.

Pressure Measurements

The internal pressure transducers used were conventional 0.635-cm microphones with pressure response cartridges. To avoid direct exposure of the microphone to the combustion gases, they were mounted outside the ducted combustion rig, and the fluctuating pressure in the rig was transmitted to the transducers by means of a "semi-infinite" acoustic waveguide. Details of these probes are given in references 42 and 43.

Temperature Measurements

The dynamic temperature fluctuations were measured with Chromel-Alumel thermocouples. The dual-thermocouple probe design shown in figure 3 was selected so that the response time of the thermocouple could be determined from the actual test data rather than from a separate precalibration. The calibration procedure discussed in reference 14 was used. The thermocouple wire diameters were 76.2 and 25.4 μm. The thermocouples were inserted into the duct by actuators after combustion started in order to prevent their destruction by the combustion startup transient.

Mean temperatures were measured at the combustor inlet and at the measurement stations in the long duct. No radial or axial temperature distribution measurements were made.

Data Acquisition and Processing

Signals from the pressure and temperature probes were simultaneously recorded on magnetic tape for later processing. Signals were recorded for 2 minutes at each operating condition. The microphones were calibrated each day with a standard pistonphone before data were recorded. The thermocouples were used simultaneously to measure mean and fluctuating temperature. The signal cross and auto spectra were obtained by off-line processing of the tape-recorded data on a two-channel fast-Fourier-transform digital signal processor with built-in analog-to-digital converters and 120-dB/octave anti-aliasing filters. The resulting spectra were then transmitted from the processor to a central computer where an analyis of the spectra produced the thermocouple calibration. Then the calibration correction was incorporated in a central computer program used to plot the data.

COMPARISON OF THEORY AND MEASUREMENTS

Measurements and theoretical calculations were made for the four test conditions shown in table I. However, similar test results were obtained at the low air mass flow rate (0.72 kg/s for inlet temperatures of 822 K (Test 115) and 1016 K (Test 116). Moreover, at the high air mass flow rate (1.54 kg/s) similar test results were obtained for inlet temperatures of 807 K (Test 117) and 667 K (Test 118). Nevertheless, for each flow, the test results were different. Consequently, only one test condition is shown at each flow rate. Since test 115 and 117 were done using similar duct inlet temperatures, these results are presented and the results for tests 116 and 118 which were similar to those for tests 115 and 117, respectively, are not shown. For each case the fuel was hydrogen gas.

At each test condition theoretical and experimental pressure auto and cross spectra are compared to check the acoustic characteristics of a particular model. Next, at each test condition theoretical and experimental temperature auto and cross spectra are compared to check the thermal characteristics of a particular model. Last, at each test condition theoretical and experimental pressure-temperature cross spectra are compared to check the source region specifications of a model. Consequently, the following six types of theoretical and experimental results are compared for each operating condition:

(1) Pressure auto spectra at the duct inlet;

(2) Pressure auto spectra at the duct exit;

(3) Pressure cross spectra between the duct inlet and the exit;

(4) Temperature cross spectra between the duct inlet and the exit;

(5) Pressure-temperature cross spectra at the duct inlet;

(6) Pressure-temperature cross spectra at the duct exit.

Furthermore, for each cross spectrum the corresponding coherence function is also presented. Note that a coherence function smaller than unity implies one or more of the following conditions exists:

(1) Extraneous noise is present in the measurements.

(2) The system relating the input to the output is nonlinear.

(3) The output is due to more than one input.

As previously discussed the zeroth-order system of equations (eqs. (11) to (13)) is solved by Runge-Kutta integration in order to establish the mean pressure, temperature, and velocity in the duct. Then, the transfer matrix equations can be used to determine the fluctuating quantities. For all the theoretical calculations the following steady-state mean volumetric-heat-flux-distribution source equation was assumed and is used in equations (11) and (12):

$$q_0 = \frac{Q_0}{\sigma\sqrt{\pi}} e^{-\left(\frac{x-x_0}{\sigma}\right)^2} + Q_1 e^{-\eta x} - 10^3(t_g - 288) \qquad (65)$$

The first term represents the heat input in the combustor. The second term represents heat addition downstream of the combustor. The third term represents heat loss through the wall of the long duct. The axial temperature distribution is not known; consequently, the parameters Q_0, Q_1, σ, and η in equation (65) are arbitrary. They are established by an iteration procedure which for each flow condition and each estimate of the parameters compares the calculated and measured temperature at the inlet and exit of the long duct. Calculations were made for cases of gradual, sharp, and small temperature rise in the combustor to the duct inlet temperature. For most comparisons of theoretical and experimental results the theoretical calculations for only the gradual and sharp temperature rise models are presented. For each temperature

rise model and at each test condition the values of Q_0 and Q_1 in equation (65) were adjusted until the calculated inlet and exit temperatures were similar to those measured using a combustor inlet temperature, t_{CIN}, of 288 K and σ values of 0.5 and 0.1. The third theoretical calculation used a combustor inlet temperature much closer to the duct inlet temperature with a σ value of 0.5. This case represents a situation where mixing of combustion gases and inlet air yields a more uniform temperature in the combustor. Again Q_0 and Q_1 were adjusted so that the measured and calculated duct inlet and exit temperatures were similar. For all cases $x_0 = 0.6$ and $\eta = 0.320$ and the measured mass flow rate was used. The parameters and resulting temperatures for each theoretical calculation are given in table II.

These three cases were selected to create examples having a sharp, a gradual, and a small temperature change in the combustor region while keeping the same temperature distribution in the long duct. Figure 4 shows the three resulting axial temperature profiles for test case 115. With $t_{CIN} = 288$ K and $\sigma = 0.5$ the temperature gradually increases to t_{INLET}. For $t_{CIN} = 288$ K and $\sigma = 0.1$ the temperature increases abruptly to T_{INLET}. For $t_{CIN} \approx t_{INLET}$ and $\sigma = 0.5$, temperature changes in the combustor section are small.

The combustor inlet reflection factor for each case was assumed to be a constant given by

$$R_{CIN} = (0.78 + i\ 0.550) \tag{66}$$

This value was selected after many trial calculations. The heat perturbation source was assumed to be near the combustor inlet.

All calculations used the same value for the fluctating heat-release rate since the major objective was to compare measured and calculated pressure-temperature cross spectra. Consequently, the pressure auto-spectra are shown without levels. The level of the spectrum changes linearly with the value of the square of the fluctuating-heat-release rate (eq. (26)). However, the selecting of the proper fluctuating-heat-release rate for a significant number of cases, finding the relation between the fluctuating-and steady-state-heat-release rates, and studying the variation of the fluctuating-heat-release rate with frequency were tasks beyond the scope of the research program.

First, acoustic and thermal theoretical and experimental results are presented to demonstrate that the the model can be used to calculate these quantities and to show that the source region model only has a secondary effect on these quantities. Then the pressure-temperature cross spectra results are presented. These show clearly the importance of the selection of of the source region model.

Pressure Auto Spectra

Measured and calculated pressure auto spectra at the duct inlet and exit for low velocity test case 115 and high velocity test case 117 are shown in figures 5 and 6. All the data presented were measured using a constant-bandwidth of 0.8 Hz. The plots show cancellations and reinforcements due to a longitudinal standing wave pattern.

Comparing calculated inlet and exit pressure spectra for t_{CIN} = 288 K and σ = 0.5 (figs. 5(b) and 6(b)) with those for t_{CIN} = 288 K and σ = 0.1 (figs. 5(c) and 6(c)) shows that the abrupt change in temperature associated with σ = 0.1 produces a spectrum that is more irregular than the spectrum associated with σ = 0.5. Using a uniform temperature profile (figs. 5(d) and 6(d)) yields a spectrum that is more damped than the spectrum associated with either σ = 0.5 or σ = 0.1. Consequently, the small temperature gradient assumption does not appear appropriate.

For all cases the measured and calculated duct inlet pressure auto spectra have cancellations at identical frequencies and the shapes of the peak at the first reinforcement are similar. Also, between 40 Hz and 200 Hz the shape of the measured and calculated peaks at the reinforcements are not similar. However, above 200 Hz the measured and calculated inlet pressure spectra again are similar.

The measured pressure spectra at the duct exit for low velocity test cases 115 (fig. 5(a)(ii)) and 116 (not shown) have similar combustion excited peaks near 120Hz which are missing in high velocity test cases 117 (fig. 6(a)(ii)) and 118 (not shown). These peaks are thought to be due a self-excited combustion noise mechanism. Except for the small combustion temperature rise case, the calculated pressure spectra at the duct exit for low velocity test cases 115 (fig. 5) and 116 (not shown) have their largest peaks at frequencies below 120 Hz while for the high velocity cases the largest peaks are at higher frequencies.

Examining the measured exit pressure spectrum shows that peaks are damped below 80 Hz for low velocity test case 115 (fig. 5(a)(ii)) and below 160 Hz for high velocity test case 117 (fig. 6(a)(ii)). The calculated exit pressure spectra do not exhibit this behavior. Finding the physical mechanism responsible for this behavior and removing this discrepancy between the measured and calculated exit pressure spectra is one of the most important tasks remaining in modeling this combustion noise data.

The calculated and measured peaks and dips in the exit pressure spectra do not match for the low velocity cases. However, they are in agreement for the high velocity cases. This type of discrepancy may be due to use of an incorrect temperature profile in the long duct. Only measurements at the inlet and exit of the long duct were used to determine the temperature profile and this may not be sufficient when combustion occurs in the long duct.

While these results show room for improvement in calculating the duct exit pressure spectra, the model does a fair job at calculating the duct inlet pressure spectra. This aspect of the calculations is important in the present paper since the objective is to compare measured and calculated pressure-temperature cross spectra at the duct inlet and to find a single model that can be used to calculate both the pressure and temperature dynamics of the system.

Pressure Cross Spectra

Measured and calculated pressure cross spectra between the duct inlet and exit are shown in figures 7 and 8 for low and high velocities (Test cases 115 and 117), respectively. The measured and calculated phase angle plots show

phase angle transitions at identical frequencies. Also, the slopes of the measured and calculated phase angle plots are similar for each case. In addition, the shapes of the first peak in the measured and calculated cross spectra are similar.

Again, the shapes of the measured and calculated peaks at the reinforcements are not similar in the frequency range from 40 to 200 Hz and are similar above 200 Hz. Comparing calculations for t_{CIN} = 288 K and σ = 0.5 with those for t_{CIN} = 288 K and σ = 0.1 shows again that the σ = 0.1 case produces a more irregular spectrum than the spectrum calculated using σ = 0.5. Although it is not shown, as with the auto spectra, the uniform (small temperature rise) combustion temperature profile assumption yields a more damped spectrum than any other case.

Temperature-temperature Coherence and Cross Spectra

The coherence between temperatures measured near the duct inlet and exit is shown in figures 9 and 10 for low velocity test case 115 and high velocity test case 117, respectively. The coherence is near 0.1 at the low frequencies. Note that spikes occur at 60 Hz indicating some electrical power line noise is present in the thermocouple signals.

Measured and calculated temperature-temperature cross spectra between the duct inlet and the exit are shown in figures 11 and 12 for test case 115 and 117, respectively. The reinforcements and cancellations predicted in the temperature cross spectra magnitude are not observable in the measurements. However, at frequencies up to 40 Hz for the low air mass flow rate case and 80 Hz for the high air mass flow rate the phase angles of both the measured and calculated results change linearly with frequency with a slope proportional to the time delay due to convection of temperature disturbances in the duct.

At frequencies above 120 Hz the magnitude is flat and the phase angle is random because the response of the thermocouples is reduced so much that the signals are at the level of the system electronic noise. In the corresponding uncompensated cross spectrum (not shown) the magnitude at 120 Hz is 40 dB down from its peak value.

The lack of signal causes the coherence shown in figures 10 and 11 to be very small above 120 Hz. The measured phase angles shown in figures 11(a) and 12(a) are more erratic when the coherence is small. Note, however, that at coherence values greater than 0.01 good phase angle values are obtained.

Pressure Temperature Coherence and Cross Spectra

The pressure-temperature coherence at the duct inlet is shown in figures 13 and 14 for test cases 115 and 117, respectively. As just noted, at low frequencies the coherence is large enough (above 0.01) so that the cross spectra phase angle measurements will be valid. This can also be inferred from a comparison of the phase angle plots shown in figures 15 and 16 and the corresponding coherence plots. Again, the pressure-temperature cross spectra phase angle values are more erratic when the coherence is small.

Measured and calculated pressure temperature cross spectra at the duct inlet are shown in figures 15 and 16 for test case 115 and 117, respectively. The locations of the cancellations in the measured and calculated cross spectra magnitude plots are similar. However, the shapes of the peaks near the reinforcements are not similar. The cross spectra phase angle plots are similar below 160 Hz. for the low air mass flow rate case and below 200 Hz for the high air mass flow rate case.

Pressure temperature coherence plots at the duct exit are shown in figures 17 and 18 for test case 115 and 117, respectively. At most points the coherence is so low that the cross spectra phase angle measurements are not reliable.

Measured and calculated pressure temperature cross spectra at the duct exit are shown in figures 19 and 20 for test cases 115 and 117, respectively. At most points the correspondence between the calculated and measured cross spectra shown in figures 19 and 20 is negligible.

The phase angle relationship is controlled by the convective velocity and the speed of sound along the duct. Both quantities are temperature dependent and thus the convective velocity and speed of sound are functions of the temperature distribution. The theoretical pressure-temperature cross spectra near the duct inlet obtained for a gradual temperature change rather than an abrupt temperature change show the best agreement with the measurements at the higher air mass flow rates (fig. 16(b)). However, at the lower air mass flow rates the uniform (small temperature rise) combustor temperature profile model calculations yields the best agreement (fig. 15(d)). Since these results indicate that the small temperature rise model is best for the pressure temperature cross spectra at the low flow rate, while the pressure auto-spectra calculations (fig. 6(d)) indicate it is not, the overall physical model is least successful for the low velocity cases.

The theoretical calculations show that at a given air mass flow rate the amount and slope of the temperature change in the source region determines the pressure-temperature phase angle variation and is more important than the inlet and exit temperatures in determining the phase angle curve shape. This behavior is in good agreement with the measured pressure-temperature phase angle plots.

These results show that the model, which explicitly links dynamic-volumetric-heat-source fluctuations to pressure and temperature fluctuations, is in good agreement with the measurements made at the higer flow rate. The correlation of combustion noise measurements with a single parameter related to the heat-release rate that can be calculated from the steady state operating conditions and the geometry, thus in effect,links the steady-state volumetric heat-release rate and the dynamic-heat-source fluctuations. The pressure-temperature cross spectra shown in figures 15 and 16 show, on a theoretical basis rather than from a statistical one, that a definite physical relationship between the pressure and the heat source exists. These results also indicate that the physical mechanism of interest involves the steady-state heat flux and the dynamic fluctuating heat input. In other words, the many correlations that have been developed that link combustion noise and heat flux are actually relations between the steady-state volumetric heat-flux and the dynamic volumetric fluctuating-heat input.

CONCLUSIONS

A one dimensional treatment of unsteady pressure and temperature disturbance generation and propagation in a combustion duct has been described. Equations that include a dynamic-volumetric-disk-heat-flux-rate source and a spatially distributed steady-state volumetric-heat-flux rate are derived.

The equations were solved by matrix methods. Good agreement was obtained between the measurements and the calculations for the higher of the two air mass flow rates used (1.57 kg/s). The results show that combustion noise is caused by fluctuating volumetric-heat-flux rate. Improved results might be obtained if more were known about the spatial distribution of the steady-state volumetric-heat-release rate, the acoustic impedance boundary conditions at the combustor inlet and duct exit, self-excited combustion noise, and the physical mechanism that damps the duct exit pressure spectrum at the low frequencies.

The use of the dynamic themocouple data does provide enough new information to suggest that the model used gives predictions that are accurate enough for practical purposes, provided the frequency of interest is low enough so that only the plane wave propagates.

The results show that correlations between parameters related to the steady state volumetric-heat-release rate and combustion noise are probably more correctly described as correlations between the steady-state volumetric-heat-flux rate and the dynamic fluctuating-volumetric-heat-flux rate. The experimental and theoretical results shown here demonstrate the physical link between the fluctuating volumetric-heat-release rate and combustion acoustics. Consequently, the combustion noise mechanism that should be investigated to better understand combustion noise involves the steady and dynamic volumetric-heat-flux rate in various combustors.

REFERENCES

1. A. A. Putnam and L. Faulkner, "An overview of combustion noise," AIAA-82-0927 (June 1982).
2. L.L. Faulkner and A. A. Putnam, "Noise control in combustion systems," Noise-Con 83, (Noise Control Foundation, New York, 1983) paper 21.4, pp. 397-406.
3. U. von Glahn and D. E. Groesbeck, "Comparison of predicted engine core noise with proposed FAA helicopter noise certification requirements," NASA TM 81739 (1981).
4. U. H. von Glahn and D. E. Groesbeck, "Comparison of predicted engine core noise with current and proposed aircraft noise certification requirements," NASA TM 82659, AIAA 81-2053 (October 1981).
5. M. Reshotko and A. Karchmer, "Core noise measurements from a small, general aviation turbofan engine," NASA TM 81610 (1980).
6. A. Karchmer, "Conditioned pressure spectra and coherence measurements in the core of a turbofan engine," AIAA-81-2052 (October 1981).
7. A. Karchmer, "Acoustic modal analysis of a full scale annular combustor," AIAA-83-0760 (April 1983).
8. E. A. Krejsa and A. M. Karchmer, "Acoustic modal analysis of the pressure field in the tailpipe of a turbofan engine," NASA TM 83387 (1983).

9. E. A. Krejsa, "New technique for the direct measurement of core noise from aircraft engines," AIAA Paper 81-1587 (July 1981).
10. U. von Glahn and E. A. Krejsa, "Correlation of core noise obtained by three signal coherence techniques," NASA TM 83012 (November 1982).
11. E. A. Krejsa, "Application of 3-signal coherence to core noise transmission," (April 1983).
12. J. H. Miles and C. A. Wasserbauer, "Analysis of Combustion Spectra Containing Organ Pipe Tones by Cepstral Techniques," NASA TM 83034 (1982).
13. J. H. Miles, C. A. Wasserbauer, and E. A. Krejsa, "Cross spectra between temperature and pressure in a constant area duct downstream of a combustor," AIAA 83-0762 (April 1983).
14. J. H. Miles, C. A. Wasserbauer, and E. A. Krejsa, "Cross spectra between pressure and temperature in a constant area duct downstream of a hydrogen fueled combustor," NASA TM 83463 (1983).
15. R. G. Huff, B. J. Clark, and R. G. Dorsch, "Interim prediction method for low frequency core engine noise," NASA TM X-71627 (Nov. 1974).
16. U. H. von Glahn, "Correlation of combustor acoustic power levels inferred from internal fluctuating pressure measurements," NASA TM-78986 (1978).
17. W. C. Strahle and M. Muthukrishnan, "Correlation of Combustor rig sound power data and theoretical basis or results," AIAA J., 18, 269-274, (1980).
18. M. R. Fink, "Experimental evaluation of theories for trailing edge and incidence fluctuation noise," AIAA J. 13, 1472-1477 (1975).
19. J. H. Miles and D. D. Raftopoulos, "Spectral structure of pressure measurements made in a combustion rig," J. Acoust. Soc. Am., 68, 1711-1722 (1980).
20. J. H. Miles and D. D. Raftopoulos, "Pressure spectra and cross spectra at an area contraction in a ducted combustion system." NASA TM 81477.
21. J. H. Miles, "Acoustic transmission matrix of a variable area duct or nozzle carrying a compressible subsonic flow," J. Acoust. Soc. Am., 69, 1577-1586 (1981).
22. J. H. Miles, "Verification of a one-dimensional analysis of sound propagation in a variable are duct without flow ," J. Acoust. Soc. Am., 72, 621-624 (1982).
23. J. H. Miles and E. A. Krejsa, "Pressure transfer function of a JT15D nozzle due to acoustic and convected entropy fluctuations," J. Acoust. Soc. Am., 72, 2008-2019 (1982).
24. J. R. Mahan, "Experimental study of the thermal-acoustic efficiency in a long turbulent diffusion-flame burner," NASA CR-3725 (1983).
25. J. R. Mahan and J. D. Jones, "Recovery of acoustic source structure in a long turbulent burner from far-field sound spectra," AIAA 83-0763, (April 1983).
26. L. R. Blevins, "Design and Documentation of a Burner for Combustion Noise Studies," M. S. Thesie, Virgina Polytechnic and State University (1981).
27. J. D. Jones, "An Experimental and Analytical Study of Noise Production and Propagation in Burners," M. S. thesis, Virginia Polytechnic and State University (1982).
28. R. G. Huff, "Simplified Combustion Noise Theory Yielding a Prediction of Fluctuating Pressure Level," NASA TP 2237 (February 1984).
29. R. R. Dils, "Dynamic Gas Temperature Measurements in a Gas Turbine Transition Duct Exit," J. Eng. Power, 95, 265-277, (July 1973).
30. M. Muthukrishnan, W. C. Strahle, and D. H. Neale, "Separation of Hydrodynamic, Entropy, and Combustion Noise in a Gas Turbine Combustor," AIAA J. 16, 320-327 (1978).

31. T. G. Sofrin, and N. Riloff, Jr., "Experimental Clean Combustor Program-Noise Study," Pratt and Whitney Aircraft, East Hartford, Conn., PWA-5458 (Sept. 1976). (NASA CR-135106).
32. D. C. Mathews, N. F. Rekos, Jr., and R. I. Nagel, "Combustion Noise Investigation-Predicting Direct and Indirect Noise from Aircraft Engines," Pratt and Whitney Aircraft Group, PWA-5478, FAA-RD-77-3 (Feb. 1977).
33. A. Kapur, A. Cummings and P. Mungur, "Sound propagation in a combustion can with axial temperature and density gradients," J. Sound Vib., 25, 129-138, (1972).
34. A. Cummings, "Ducts with axial temperature gradients: an approximate solution for sound transmission and generation," J. Sound and Vib., 51, 55-67, (1977).
35. A. Cummings, "Standing wave anaysis with temperature gradients," J. Sound Vib., 51, 143-145, (1977).
36. A. Cummings, "High temperature effects on the radiation impedance of an unflanged duct exit," J. Sound Vib., 52, 299-304, (1977).
37. A. Cummings, "Sound generation and transmission in flow ducts with axial temperature gradients," J. Sound Vib., 57, 261-279, (1978).
38. J. E. Cole, III, "Sound propagation in a duct with axial sound speed variation: an exact solution," J. Sound Vib., 63, 237-246, (1979).
39. M. G. Prasad and M. J. Crocker, "Evaluation of four-pole parameters for a straight pipe with a mean flow and a linear temperature gradient," J. Acoust. Soc. Am., 69, 916-921 (1981).
40. B. Carnakan, H. A. Luther and J. O. Wilkes, Applied numerical methods (John Wiley, New York, 1969) pp. 361-379.
41. A. D. Pierce, Acoustics, (McGraw-Hill, New York, 1981), p. 222.
42. A. M. Karchmer and M. Reshotko, "Core noise source diagnostics on a turbofan engine using correlation and coherence techniques, "NASA TM X-73535 (1976).
43. A. M. Karchmer, M. Reshotko, and F. J. Montegani, "Measurement of far field combustion noise from a turbulent engine using coherence functions," AIAA Paper 77-1277 (October 1977).

TABLE I. - TEST CONDITIONS

Test condition	Test			
	115	116	117	118
Air mass flow rate, kg/s	0.72	0.73	1.54	1.55
Hydrogen mass flow rate, kg/s	0.0031	0.0043	0.0069	0.0050
Fuel-air ratio	0.0043	0.0059	0.0045	0.0030
Duct temperature, K:				
T_{inlet}	822	1016	807	667
T_{exit}	792	954	902	765

TABLE II. - THEORETICAL CALCULATIONS

Condition	Test No.											
	115			116			117			118		
	Mass flow rate, W, kg/s											
	0.72			0.73			1.54			1.55		
σ	0.5	0.5	0.1	0.5	0.5	0.1	0.5	0.5	0.1	0.5	0.5	0.1
Combustor inlet temperature, $T_{c,in}$, K	288	795	288	288	995	288	288	780	288	288	620	288
Volumetric-heat-release-rate coefficients:												
$Q_0 \times 10^6$	12.8	0.9	12.8	18.3	0.9	18.4	24	0.1	24.6	16.7	0.1	17.1
$Q_1 \times 10^6$	1.3	1.3	1.35	1.3	1.3	1.4	5.2	5.0	5.4	4.8	5.0	4.95
Duct temperature, K:												
T_{inlet}	826	826	822	1018	1013	1016	800	808	808	661	667	667
T_{exit}	795	793	792	954	946	954	892	904	902	758	766	763

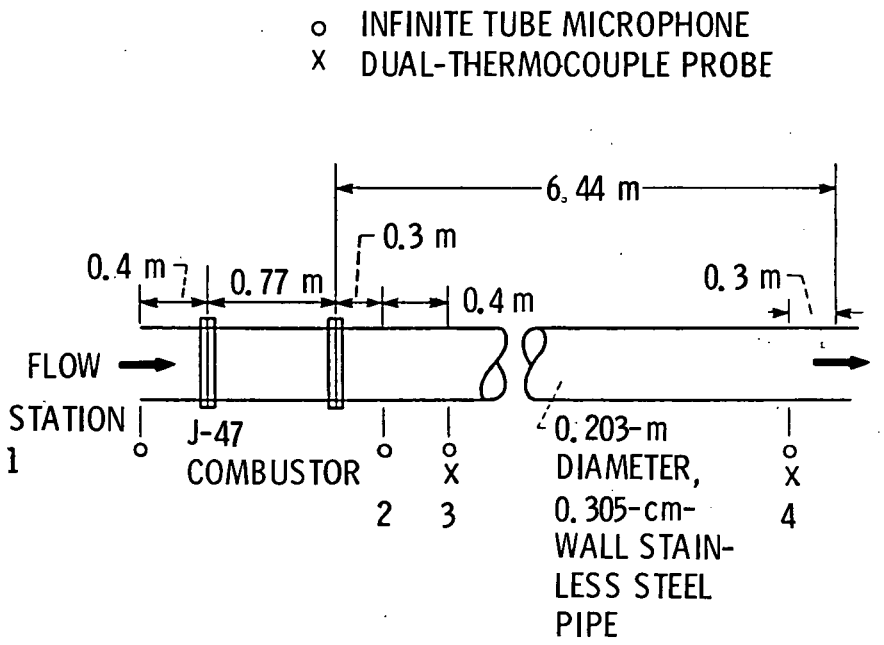

(a) RIG SCHEMATIC.

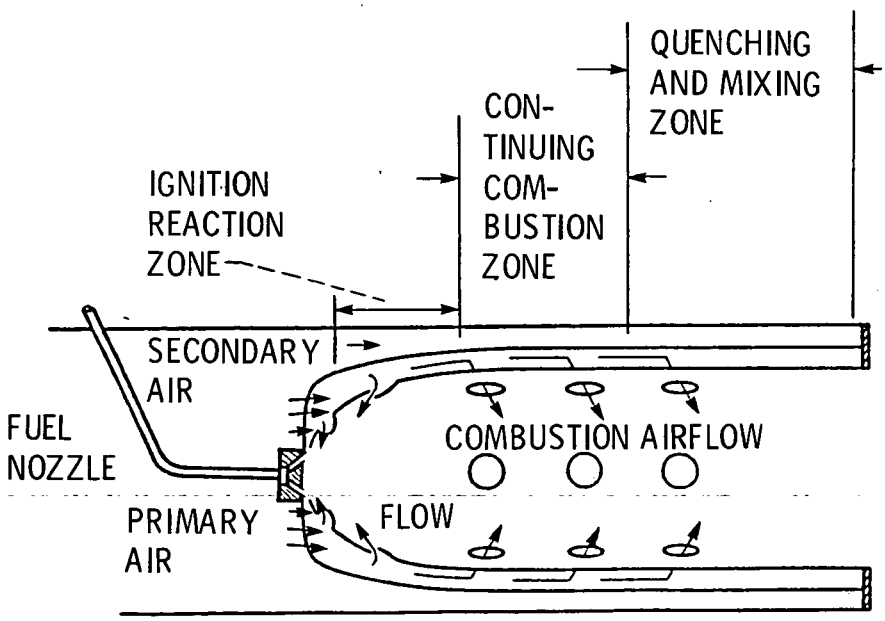

(b) INJECTION SCHEME.

Figure 1. - Schematic of ducted combustion system rig.

Figure 2. - NASA Lewis combustion acoustics facility.

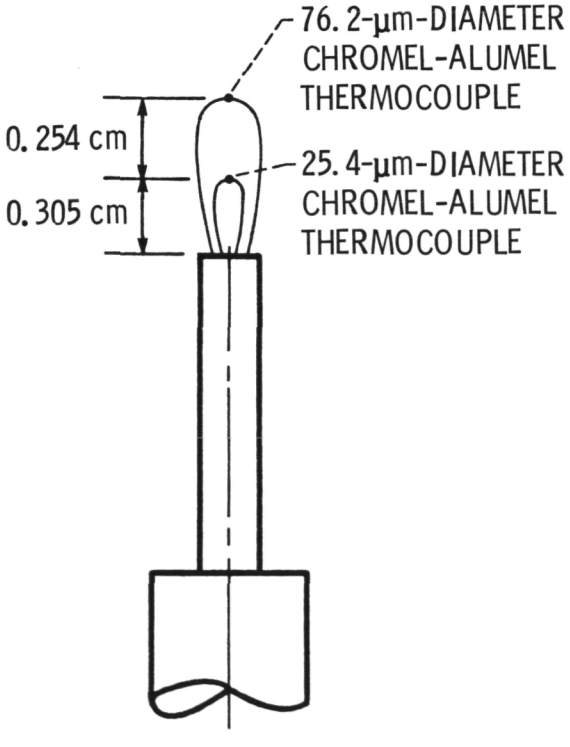

Figure 3. - Dual-thermocouple probe design.

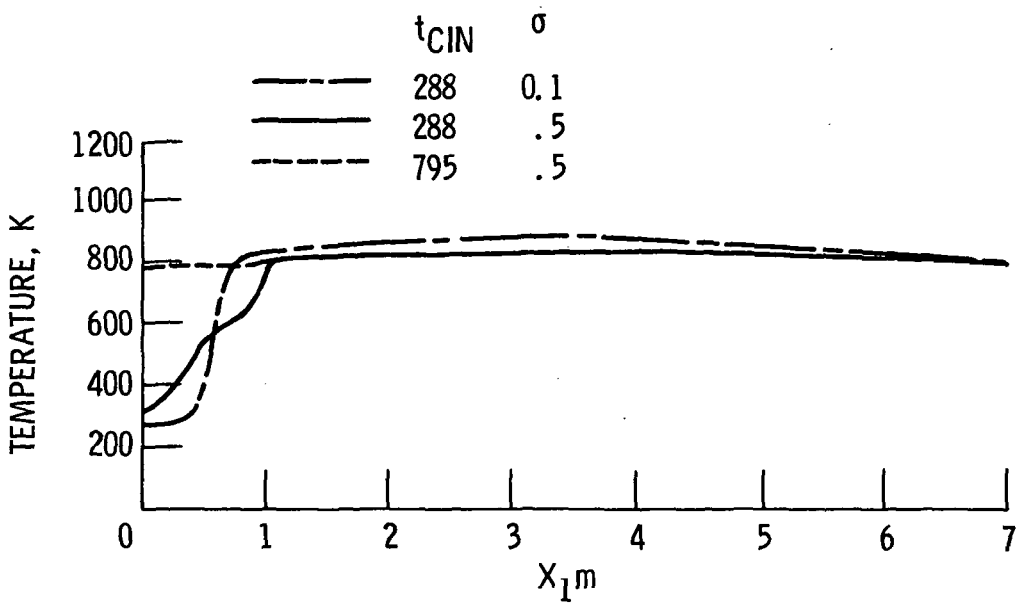

Figure 4. - Calculated duct temperature profile (test number 115 W = 0.72 kg/s).

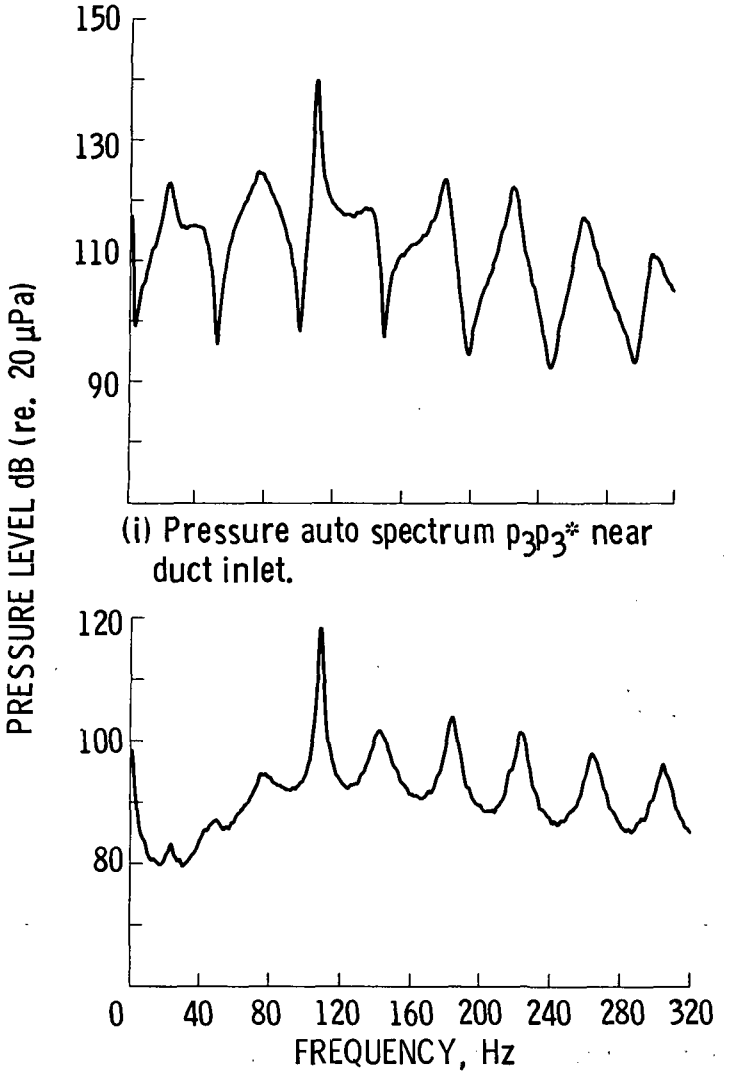

(i) Pressure auto spectrum $p_3 p_3^*$ near duct inlet.

(ii) Pressure auto spectrum $p_4 p_4^*$ near duct exit.

(a) Measured pressure auto spectra for bandwidth of 0.8 Hz.

Figure 5. - Pressure auto spectrum for test 115.

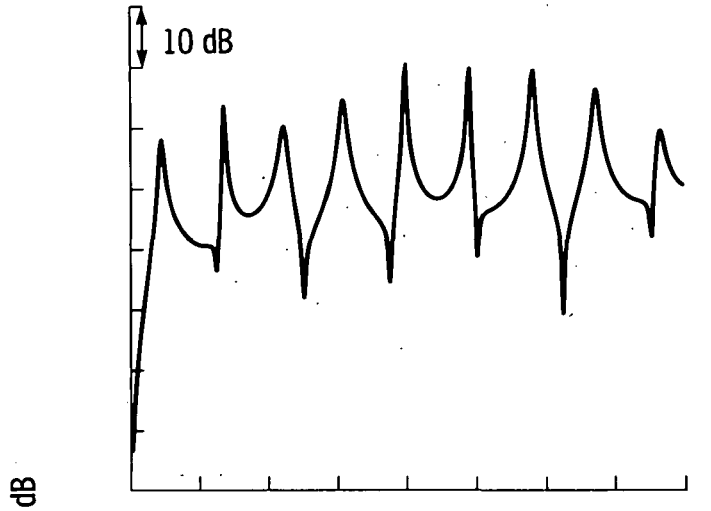

(i) Pressure auto spectrum $p_3 p_3^*$ near duct inlet.

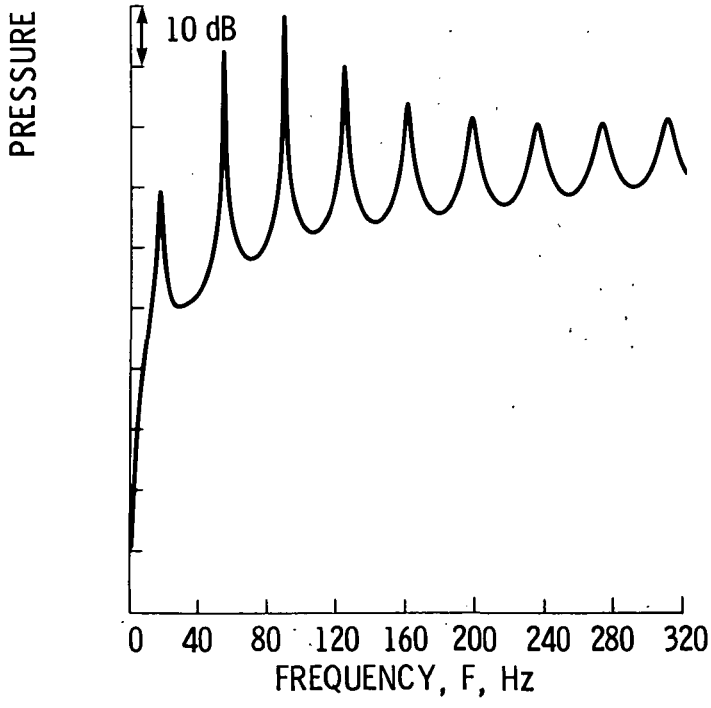

(ii) Pressure auto spectrum $p_4 p_4^*$ near duct exit.

(b) Calculated auto spectra (t_{CIN} = 288 K, σ = 0.5).

Figure 5. - Continued.

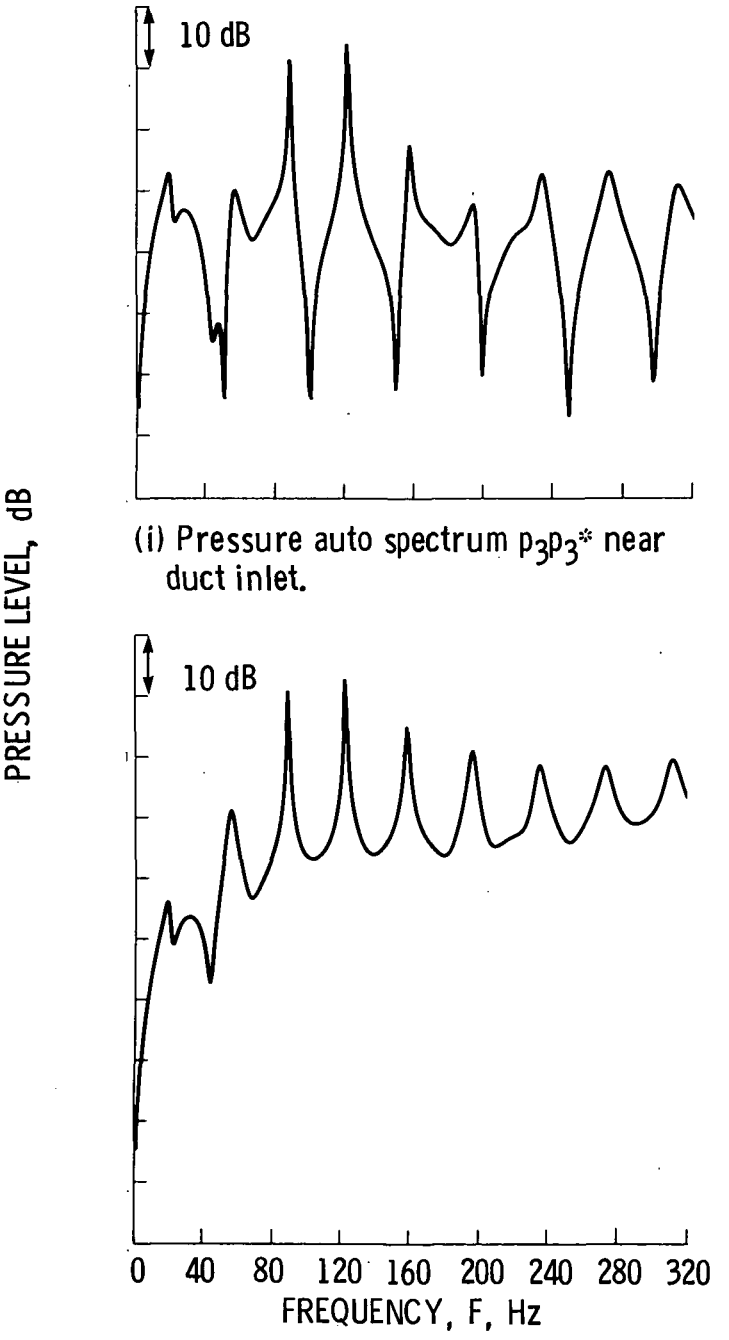

(i) Pressure auto spectrum $p_3 p_3^*$ near duct inlet.

(ii) Pressure auto spectrum $p_4 p_4^*$ near duct exit.

(c) Calculated spectra (t_{CIN} = 288 K, σ = 0.1.)

Figure 5. - Continued.

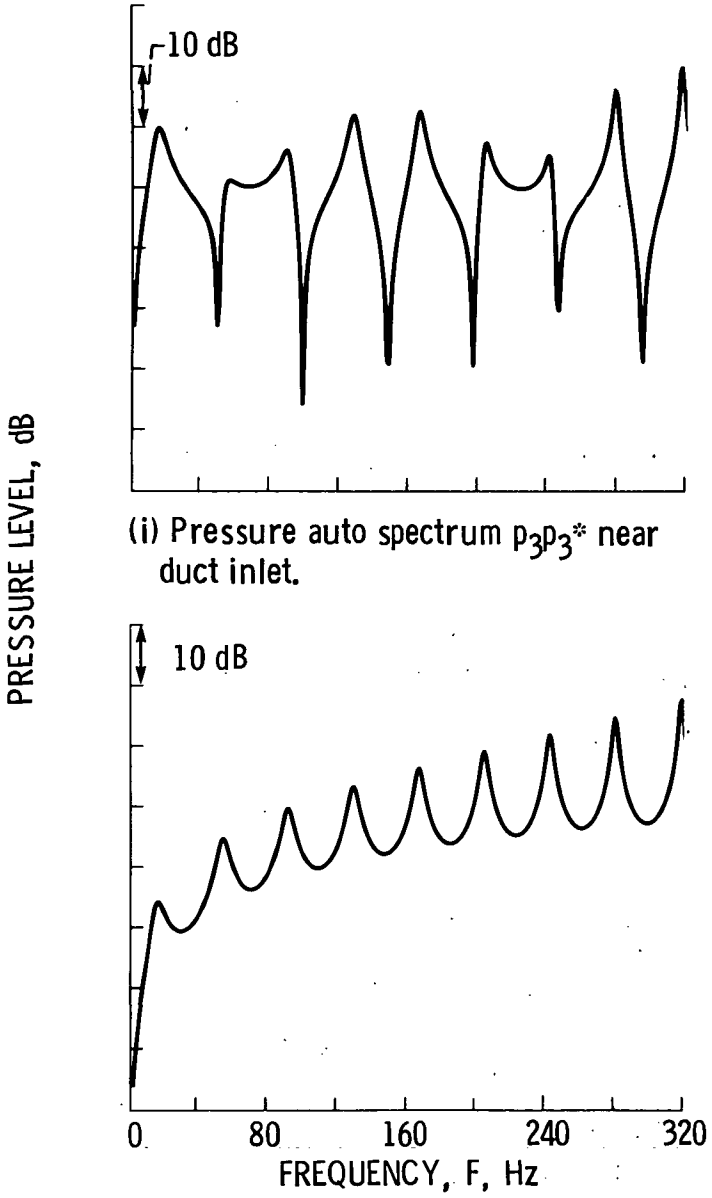

(i) Pressure auto spectrum $p_3 p_3^*$ near duct inlet.

(ii) Pressure auto spectrum $p_4 p_4^*$ near duct exit.

(d) Calculated spectrum (t_{CIN} = 795 K, σ = 0.5).

Figure 5. - Concluded.

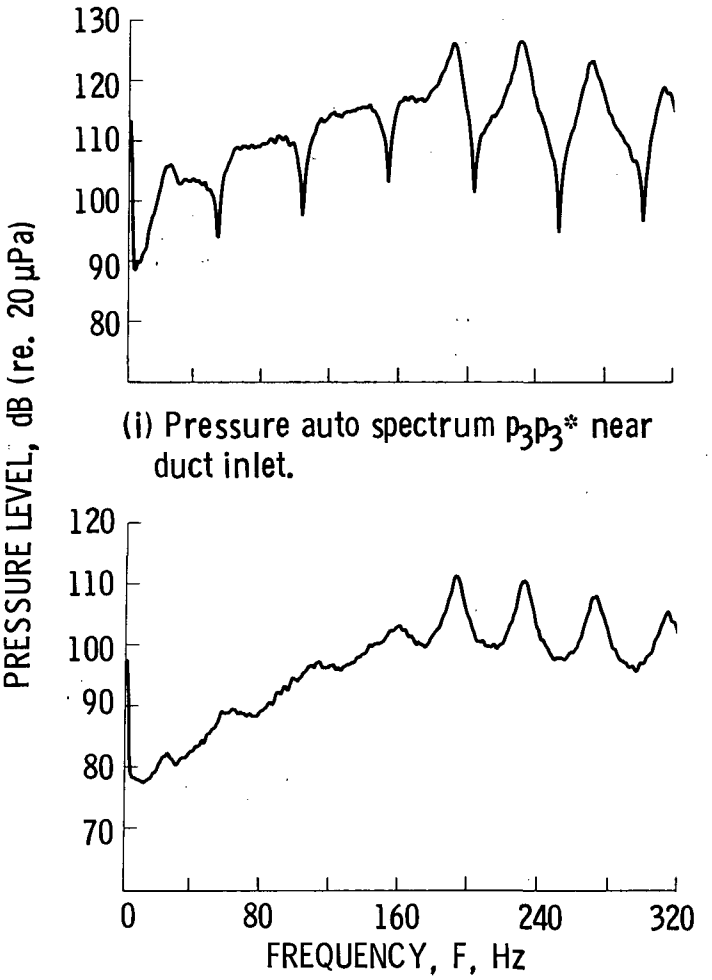

(i) Pressure auto spectrum $p_3 p_3^*$ near duct inlet.

(ii) Pressure auto spectrum $p_4 p_4^*$ near duct exit.

(a) Measured pressure auto spectra for bandwidth of 0.08 Hz.

Figure 6. - Pressure auto spectra for test 117.

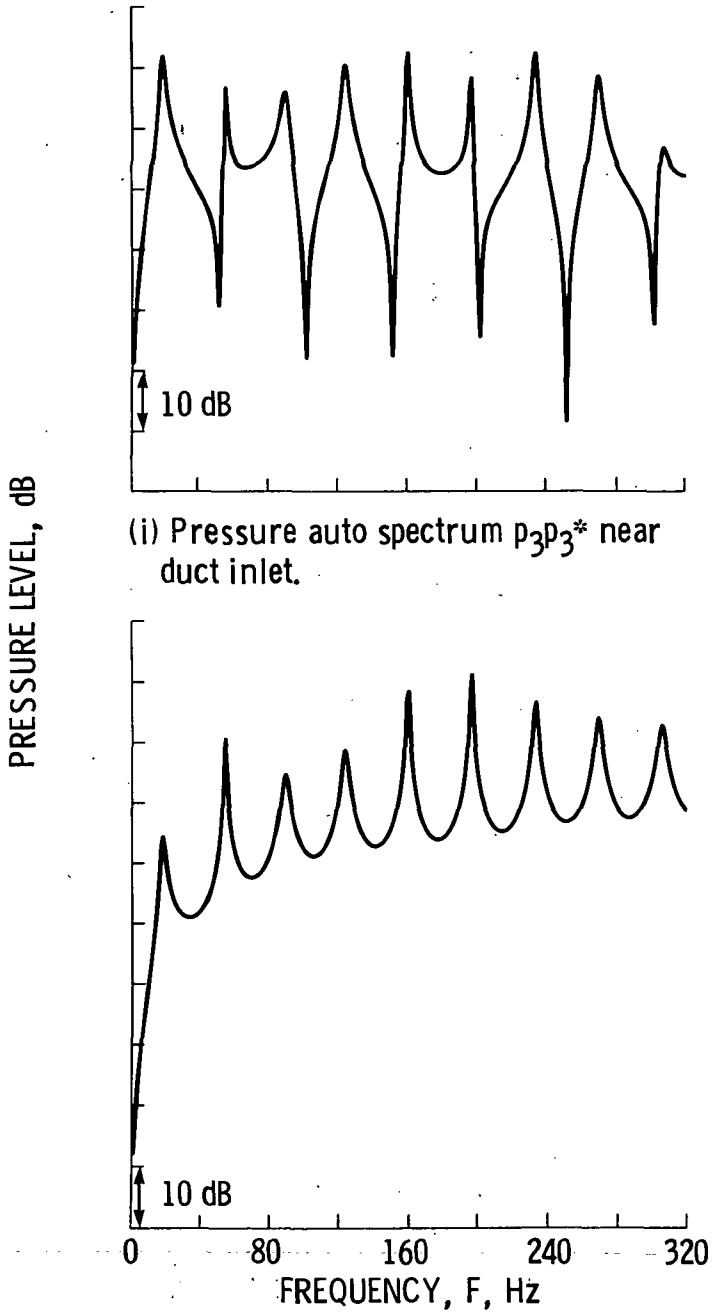

(i) Pressure auto spectrum $p_3 p_3^*$ near duct inlet.

(ii) Pressure auto spectrum $p_4 p_4^*$ near duct exit.

(b) Calculated auto spectra (t_{CIN} = 288 K, σ = 0.5).

Figure 6. - Continued.

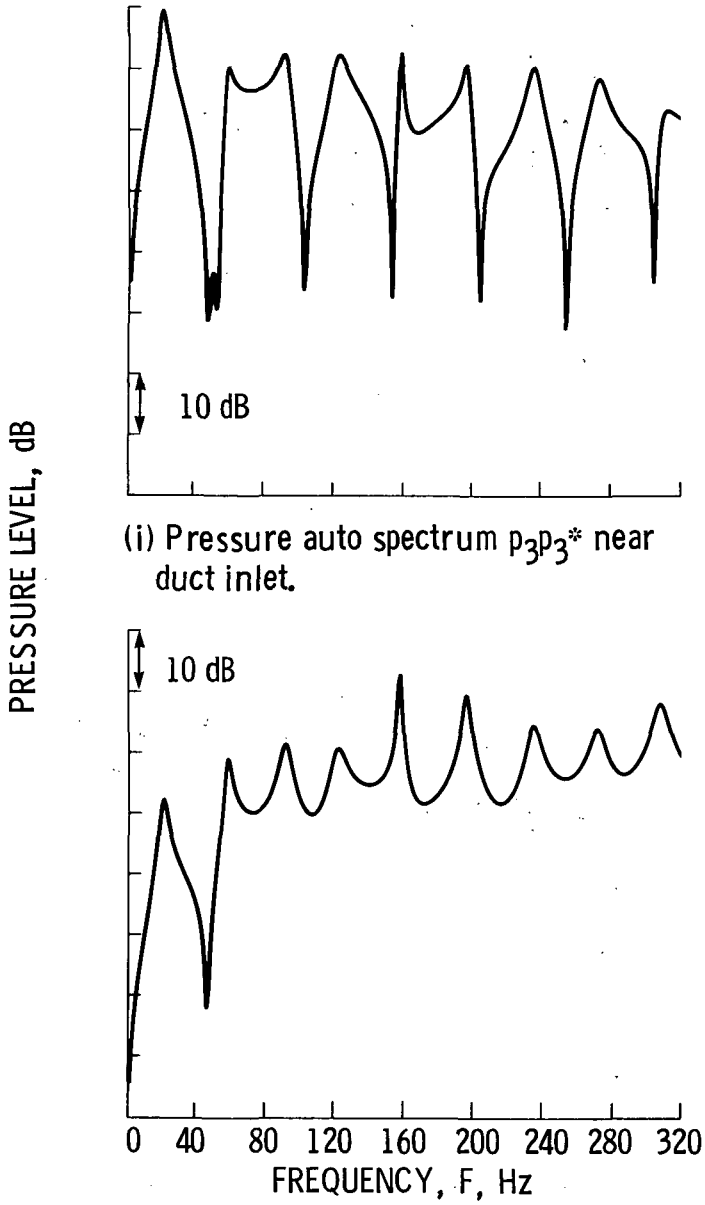

(i) Pressure auto spectrum $p_3p_3^*$ near duct inlet.

(ii) Pressure auto spectrum $p_4p_4^*$ near duct exit.

(c) Calculated auto spectra (t_{CIN} = 288 K, σ = 0.1).

Figure 6. - Continued.

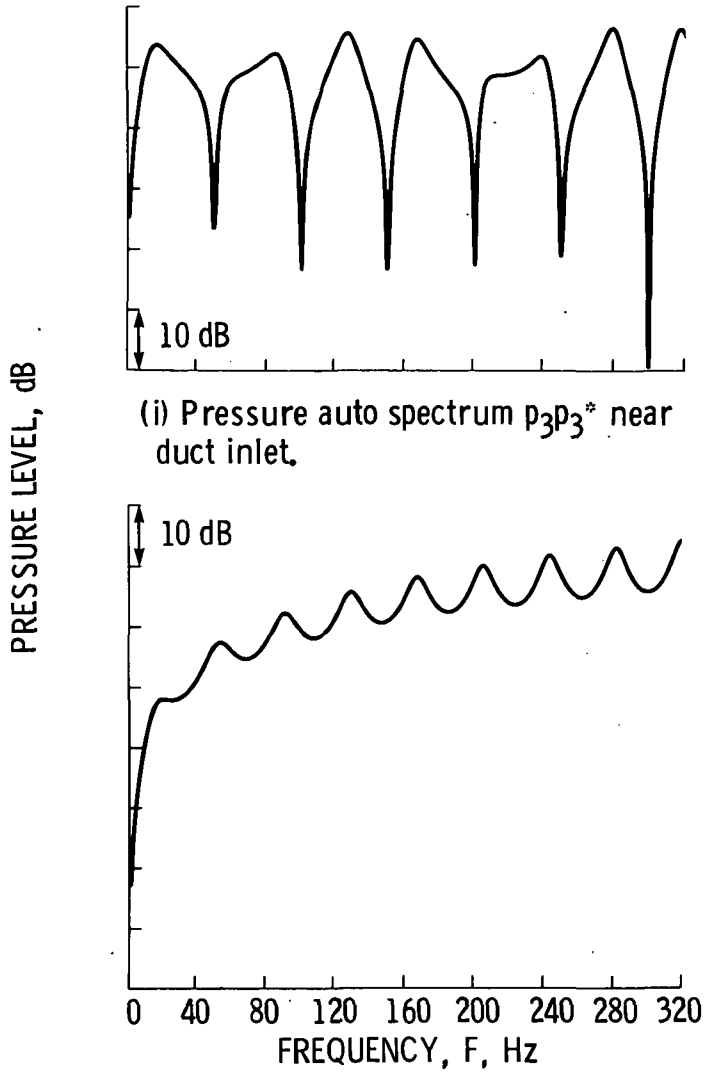

(i) Pressure auto spectrum $p_3 p_3^*$ near duct inlet.

(ii) Pressure auto spectrum $p_4 p_4^*$ near duct exit.

(d) Calculated auto spectra (t_{CIN} = 780 K, σ = 0.5).

Figure 6. - Concluded.

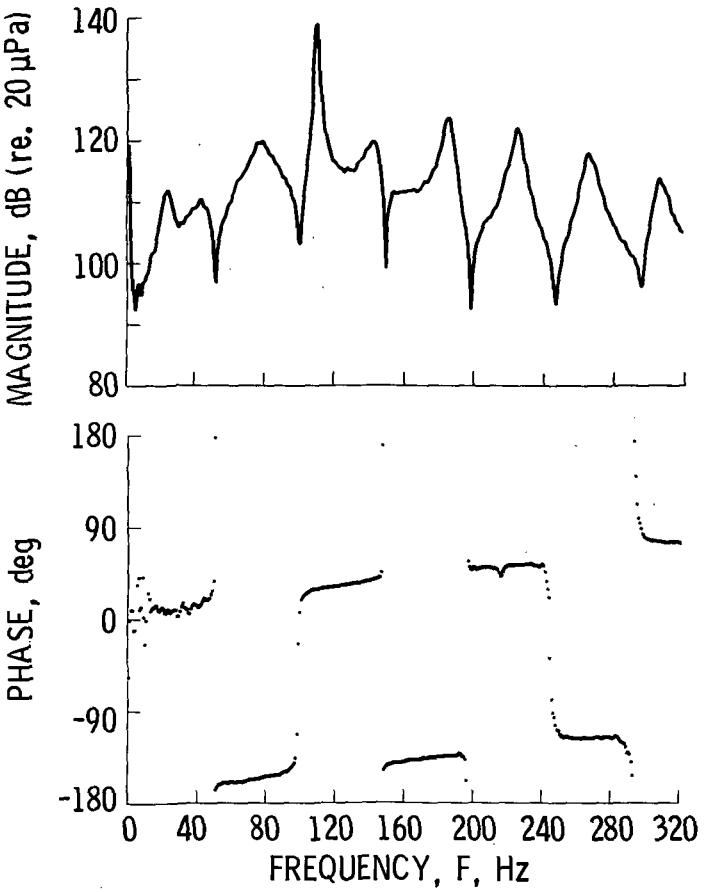

(a) Measured pressure cross spectrum $p_4 p_3^*$ for bandwidth 0.8 Hz.

Figure 7. - Pressure cross spectra between station 3 and 4 for test 115.

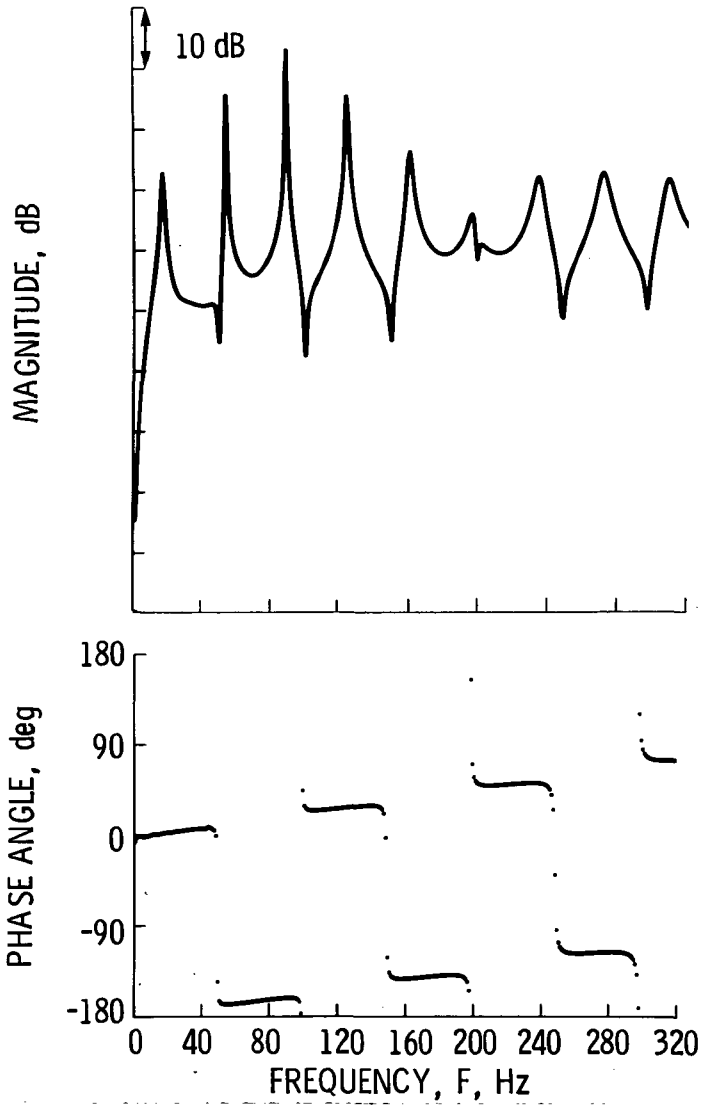

(b) Calculated pressure cross spectra $p_4 p_3^*$ (t_{CIN} = 288 K, σ = 0.5)

Figure 7. - Continued.

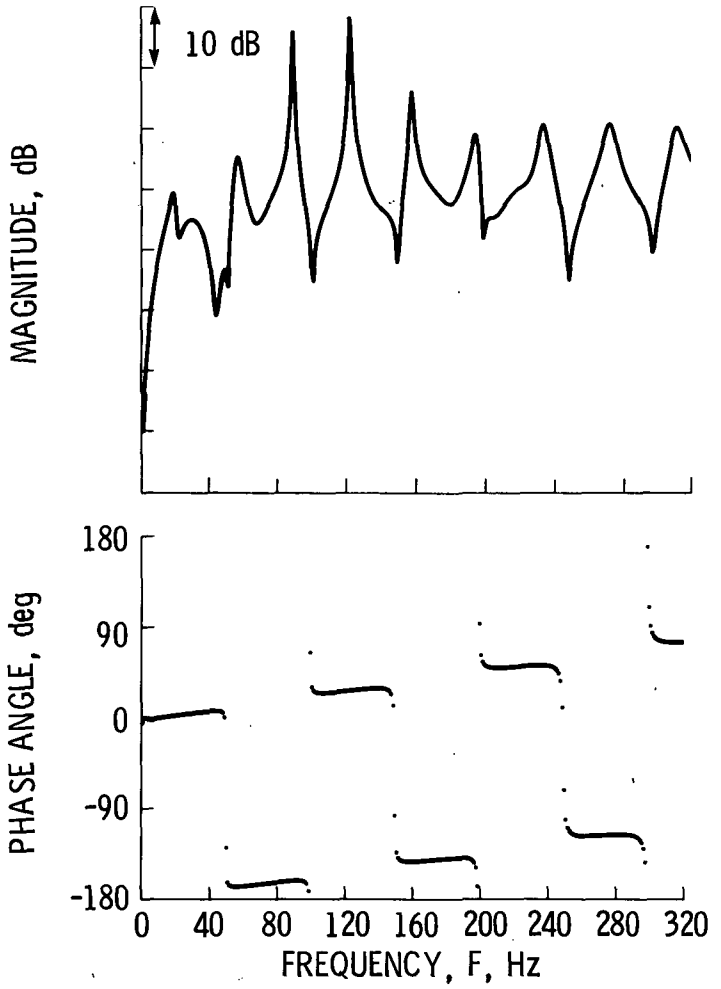

(c) Calculated pressure cross spectra $p_4 p_3^*$ (t_{CIN} = 288 K, σ = 0.1).

Figure 7. - Concluded.

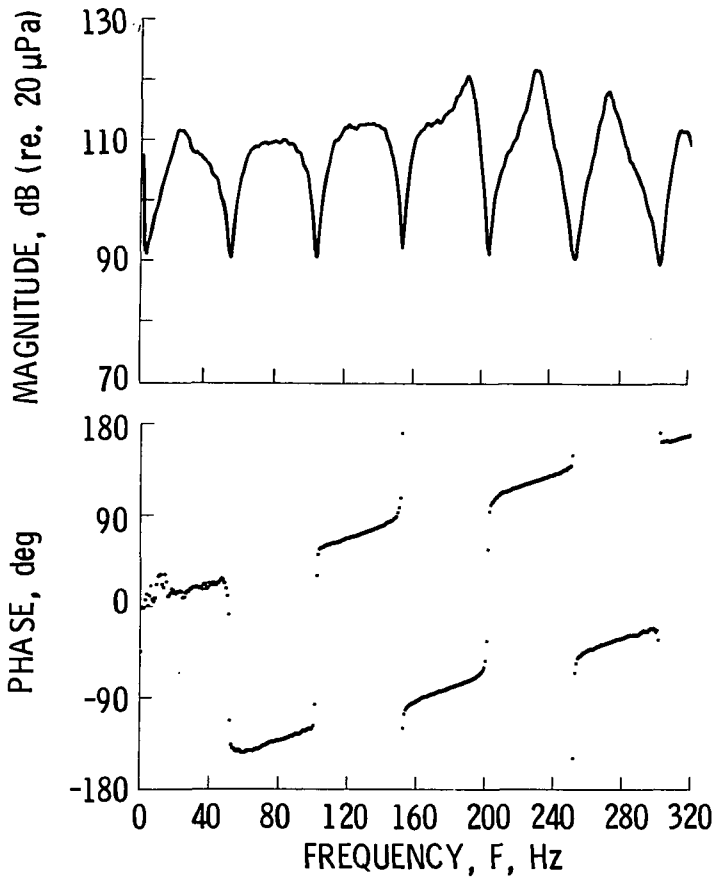

(a) Measured pressure cross spectrum $p_4 p_3^*$ for bandwidth of 0.8 Hz.

Figure 8. - Pressure cross spectra between station 3 and 4 for test 117.

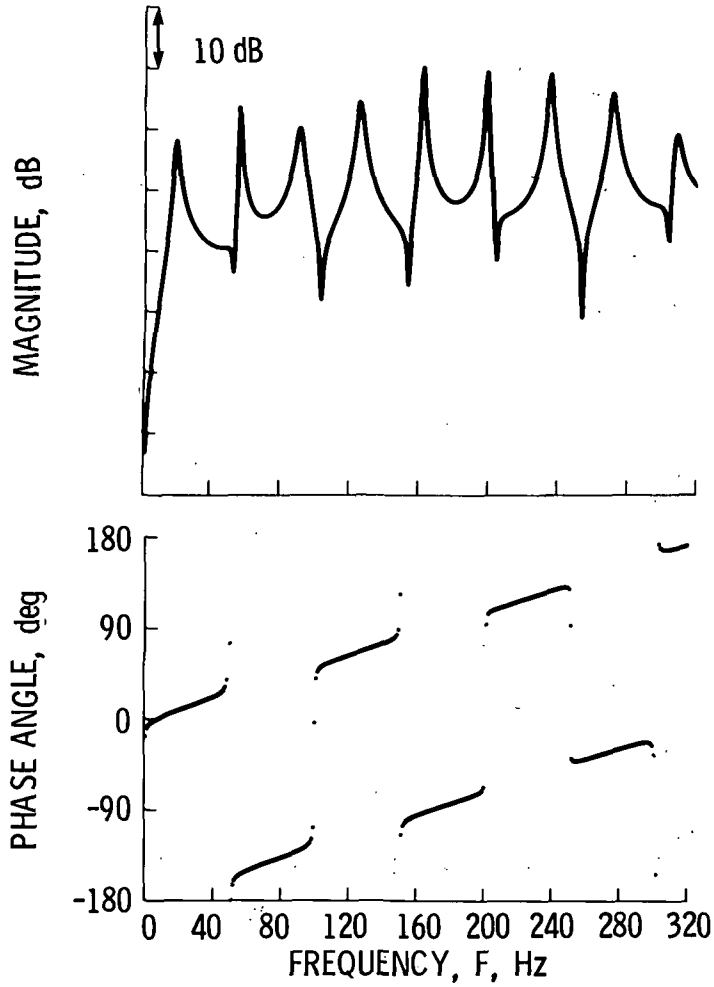

(b) Calculated pressure cross spectra $p_4 p_3^*$ (t_{CIN} = 288 K, σ = 0.5).

Figure 8. - Continued.

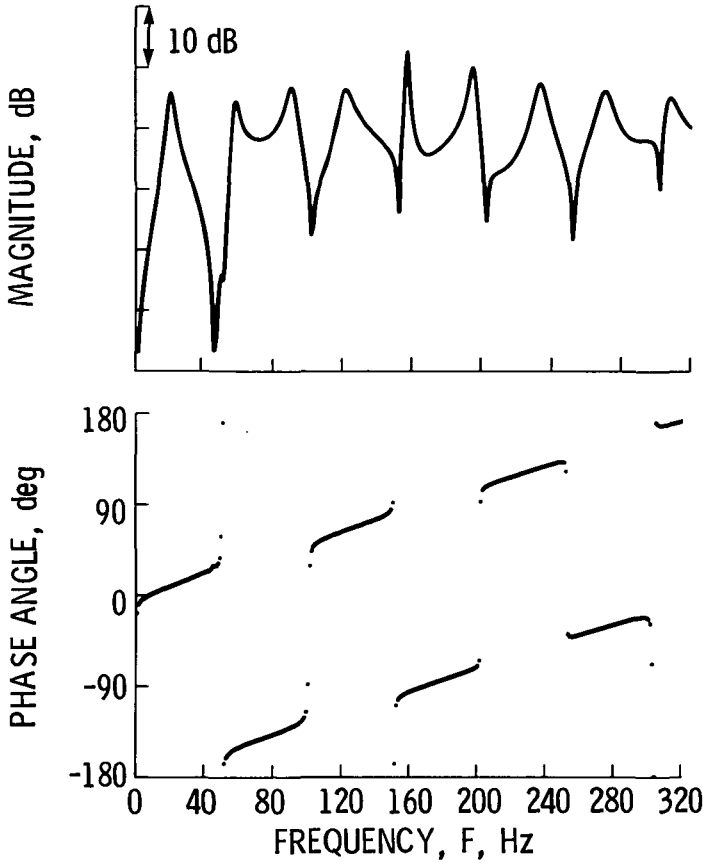

(c) Calculated pressure cross spectra $p_4 p_3^*$ (t_{CIN} = 288 K, σ = 0.5).

Figure 8. - Concluded.

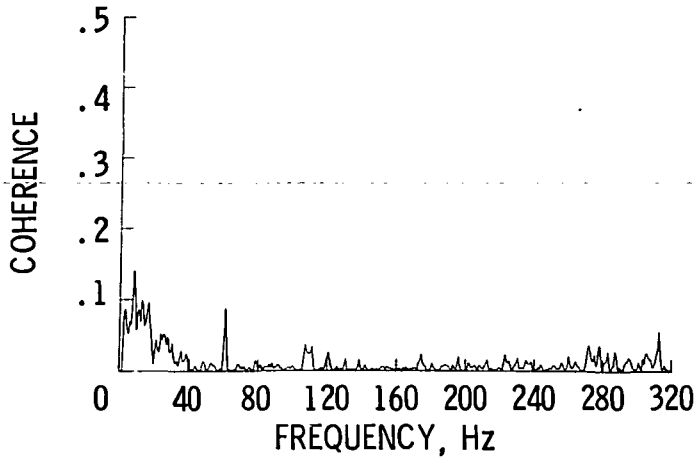

Figure 9. - Coherence between duct inlet and exit temperatures $|t_4 t_3^*|^2 / |t_4|^2 |t_3|^2$, test no. 115 (bandwidth = 0.8 Hz).

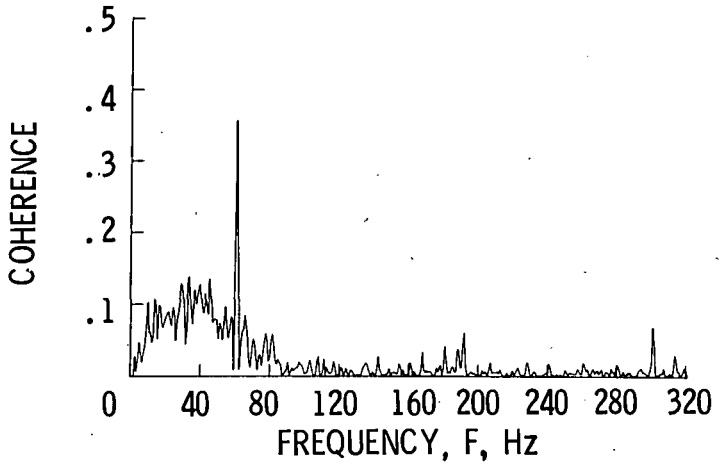

Figure 10. - Coherence between duct inlet and exit temperature $|t_4 t_3^*|^2 / |t_4|^2 |t_3|^2$ for test 117 (bandwidth = 0.5 Hz).

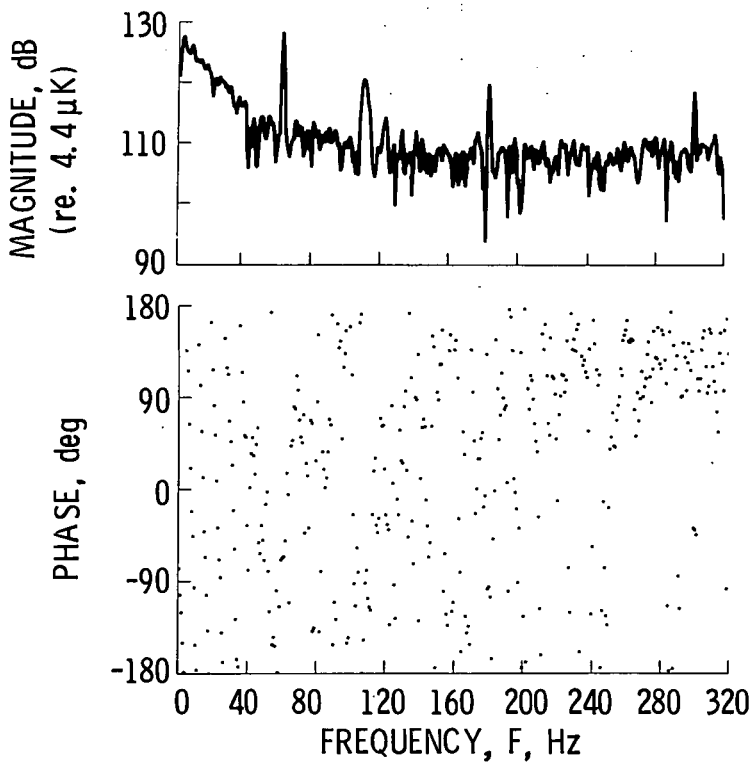

(a) Measured temperature cross spectra with a bandwidth of 0.8 Hz.

Figure 11. - Temperature cross spectra $t_4 t_3^*$ between duct inlet and duct exit for test 115.

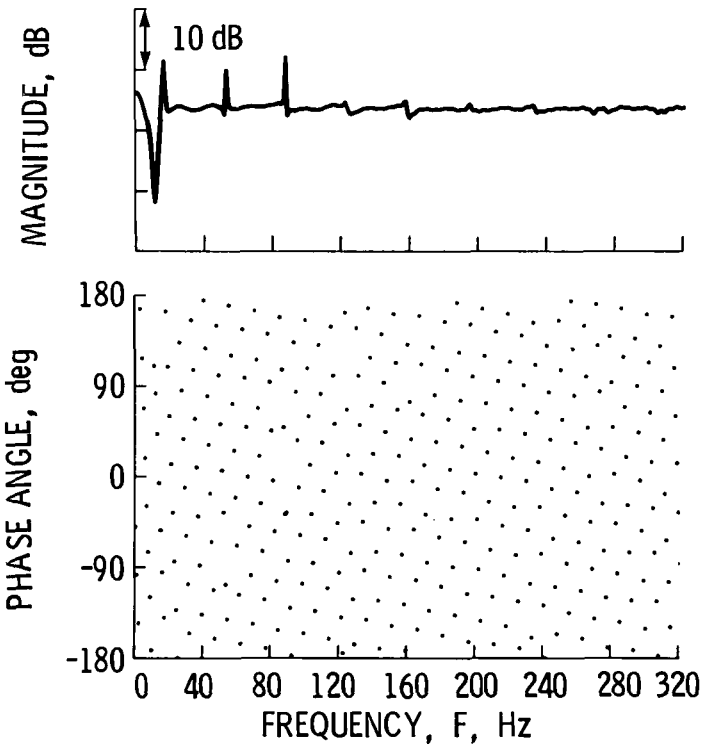

(b) Calculated temperature cross spectrum (t_{CIN} = 288 K, σ = 0.5).

Figure 11. - Continued.

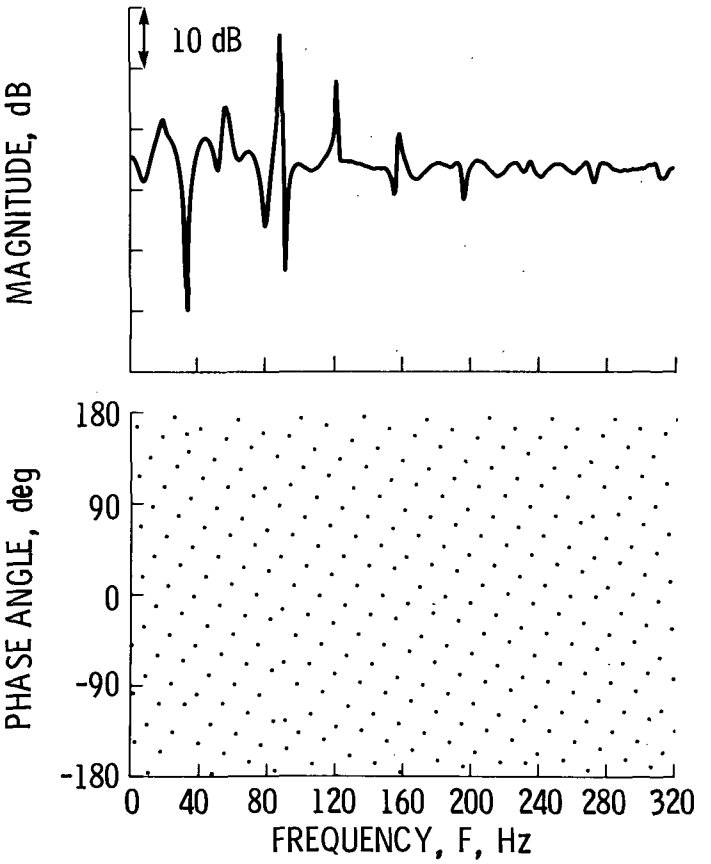

(c) Calculated temperature cross spectrum (t_{CIN} = 288 K, σ = 0.1).

Figure 11. - Concluded.

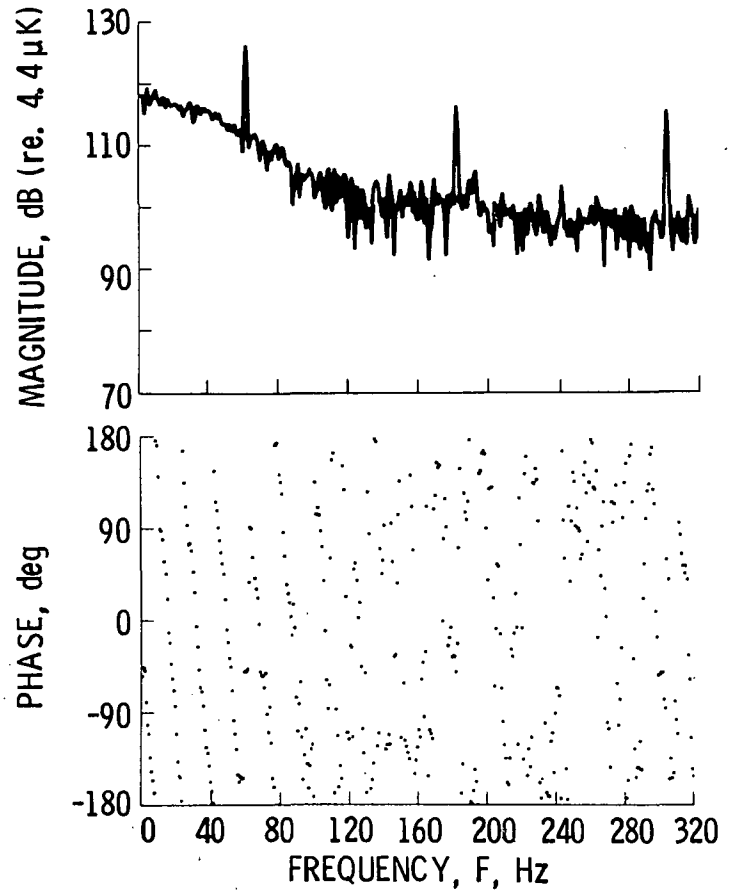

(a) Measured temperature cross spectra with bandwidth of 0.8 Hz.

Figure 12. - Temperature cross spectra $t_4 t_3^*$ between duct inlet and duct exit for test 117.

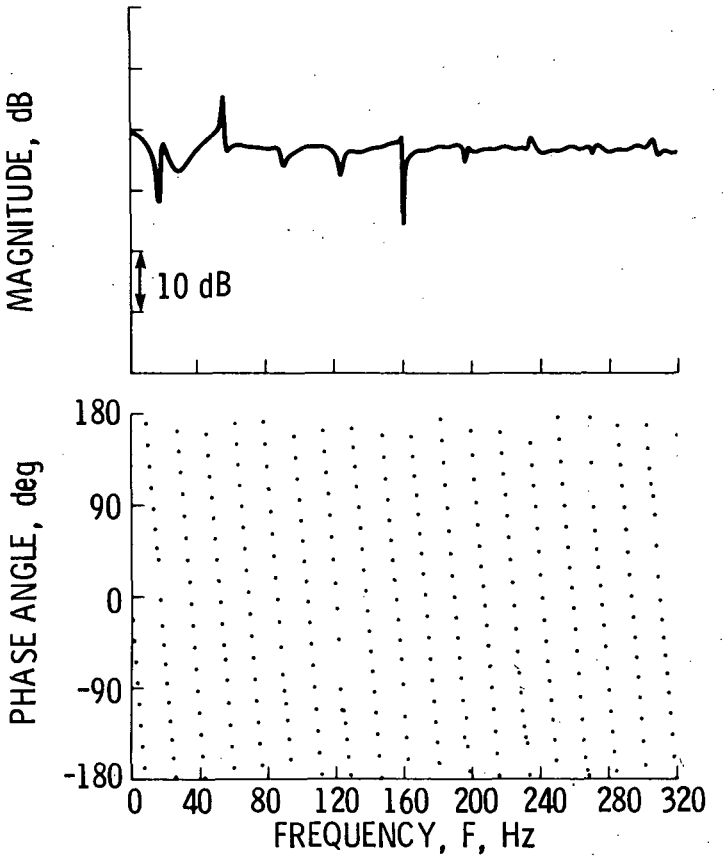

(b) Calculated temperature cross spectrum (t_{CIN} = 288 K, σ = 0.5)

Figure 12. - Continued.

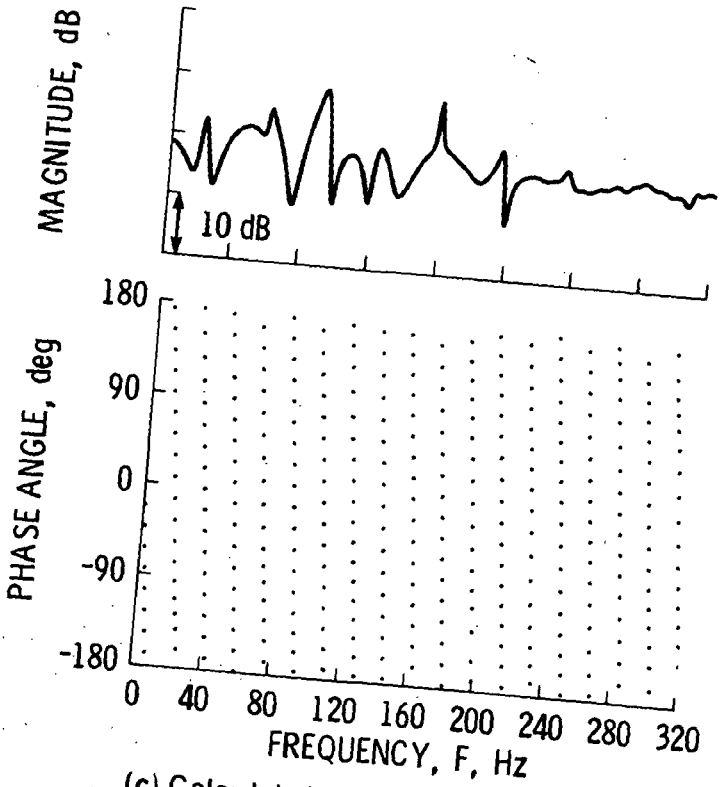

(c) Calculated temperature cross spectrum (t_{CIN} = 288 K, σ = 0.1

Figure 12. - Concluded.

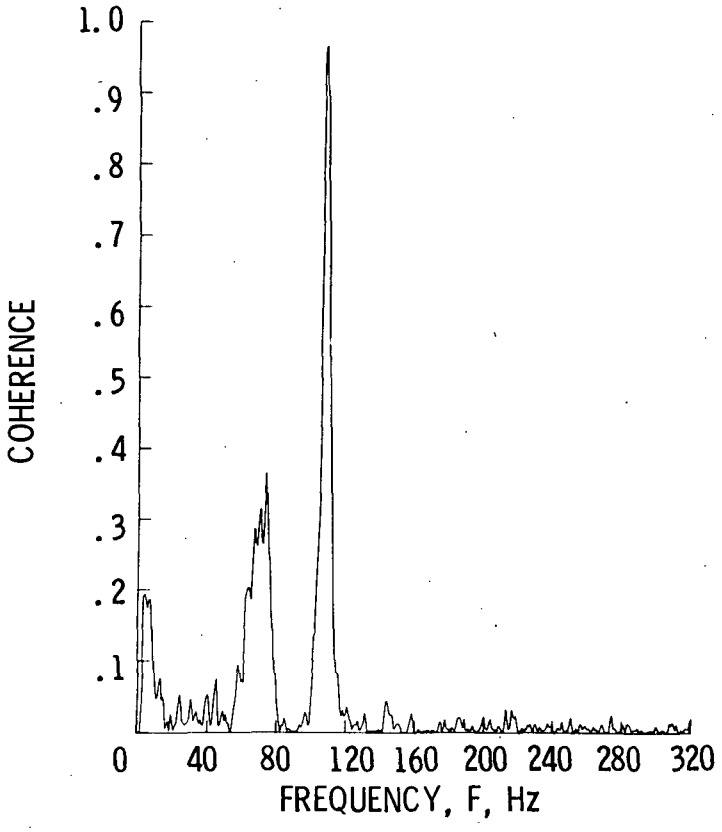

Figure 13. - Coherence between pressure and temperature at duct inlet $|p_3 t_3^*|^2 / |p_3|^2 |t_3|^2$ for test 115 (bandwidth = 0.8 Hz).

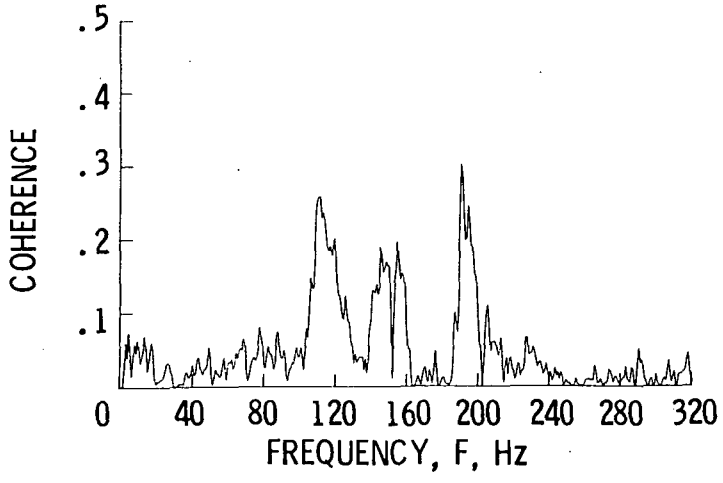

Figure 14. - Coherence between pressure and temperature at duct inlet $|p_3 t_3^*|^2 / |p_3|^2 |t_3|^2$ for test 117 (bandwidth = 0.8 Hz).

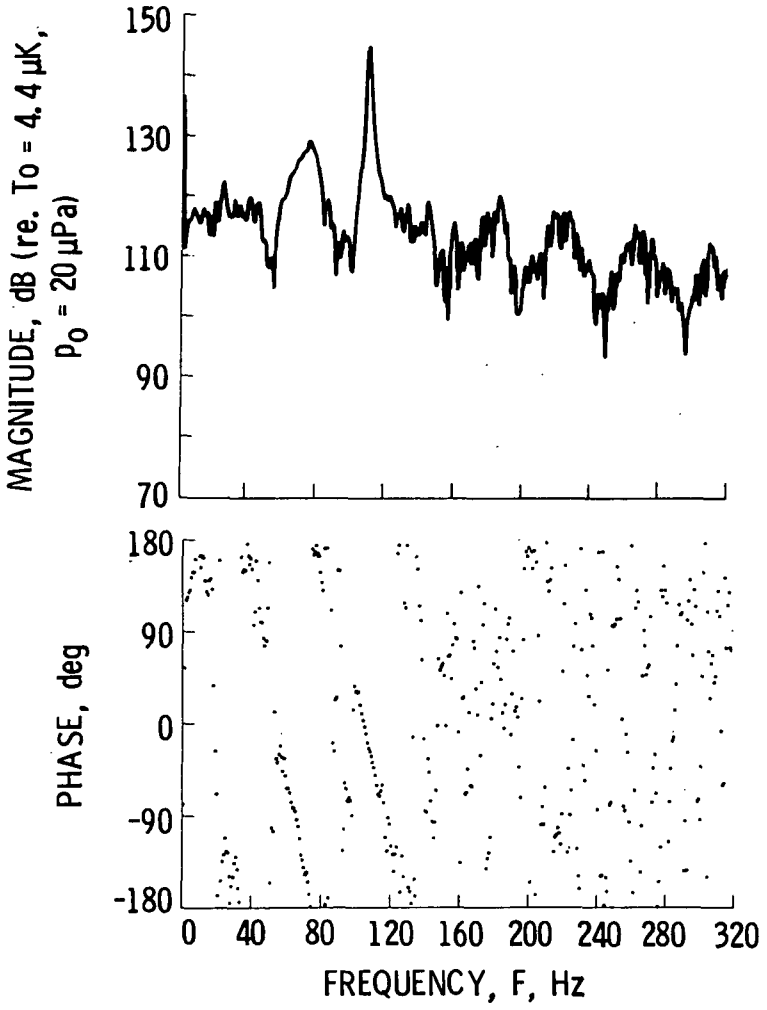

(a) Measured pressure temperature cross spectrum with a bandwidth of 0.8 Hz.

Figure 15. - Pressure temperature cross spectra near duct inlet p_3t_3* for test 115.

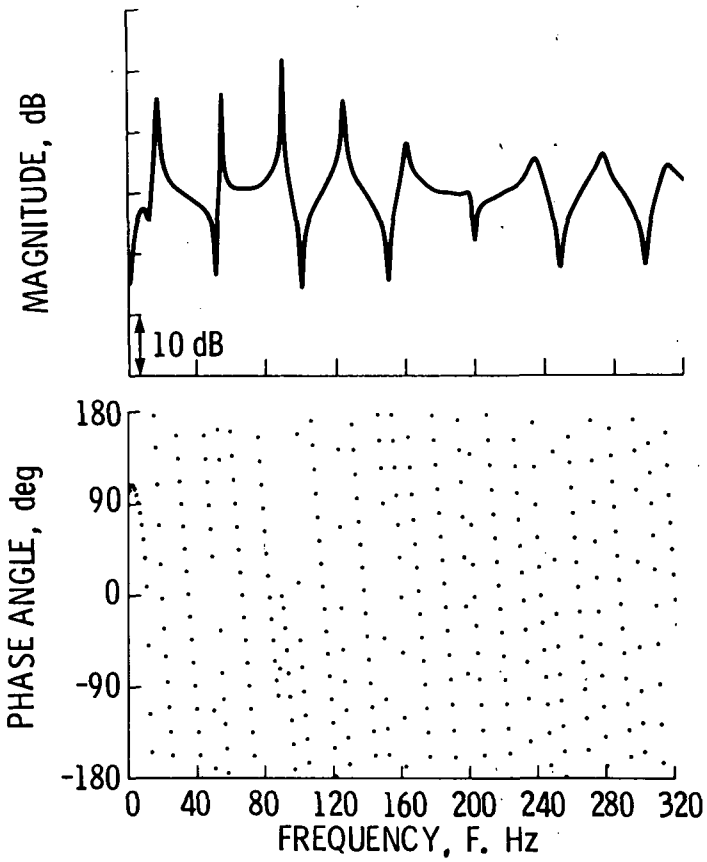

(b) Calculated pressure temperature cross spectrum (t_{CIN} = 288 K, σ = 0.5)

Figure 15. - Continued.

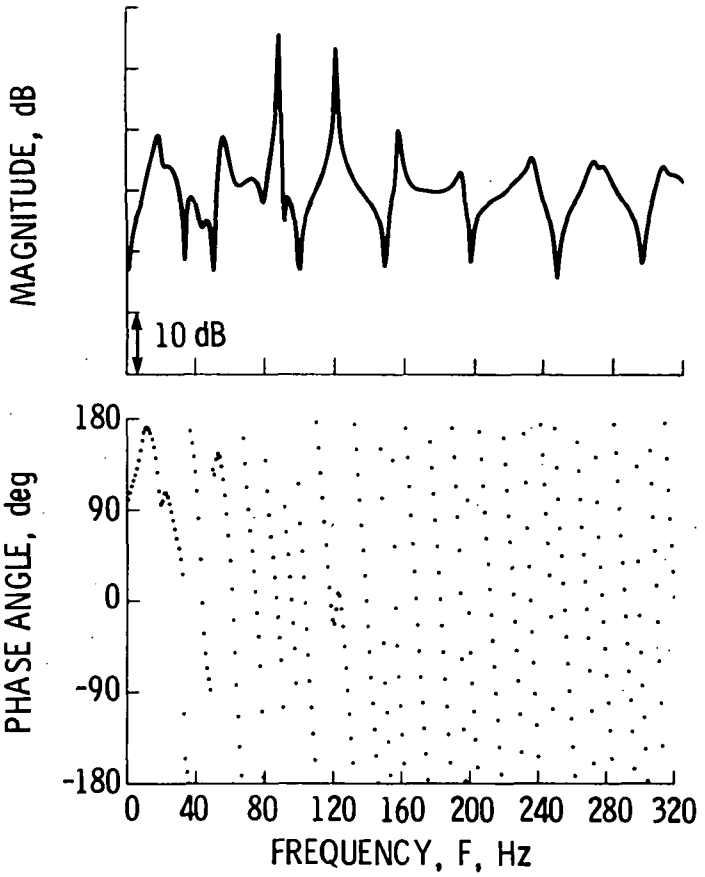

(c) Calculated pressure temperature cross spectrum (t_{CIN} = 288 K, σ = 0.1).

Figure 15. - Continued.

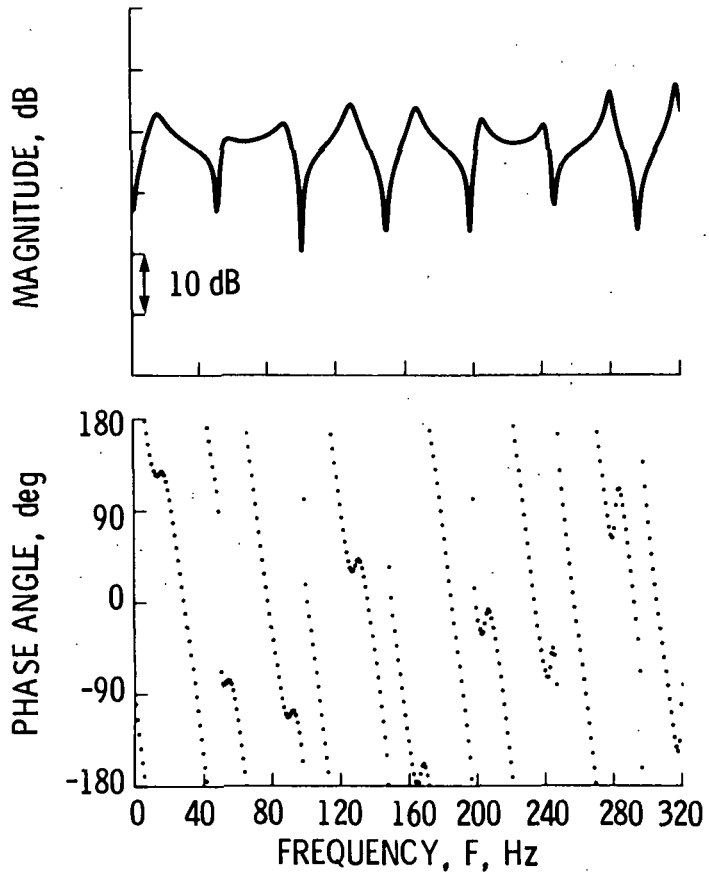

(d) Calculated pressure temperature cross spectrum (t_{CIN} = 795 K, σ = 0.5).

Figure 15. - Concluded.

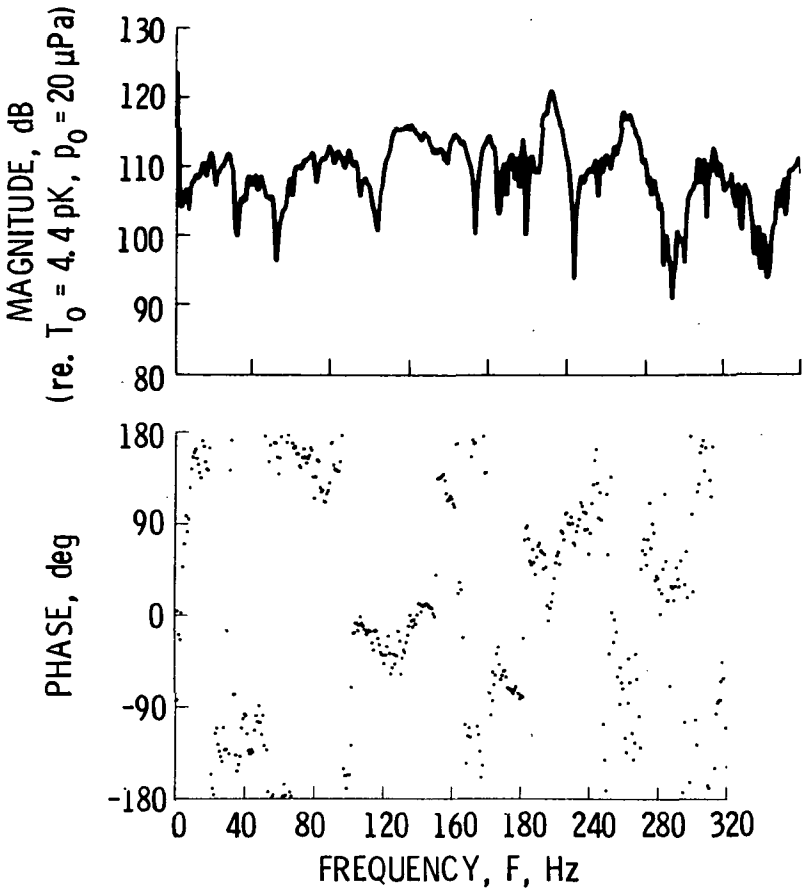

(a) Measured pressure temperature cross spectrum with a bandwidth of 0.8 Hz.

Figure 16. - Pressure temperature cross spectra near duct inlet p_3t_3* for test 117.

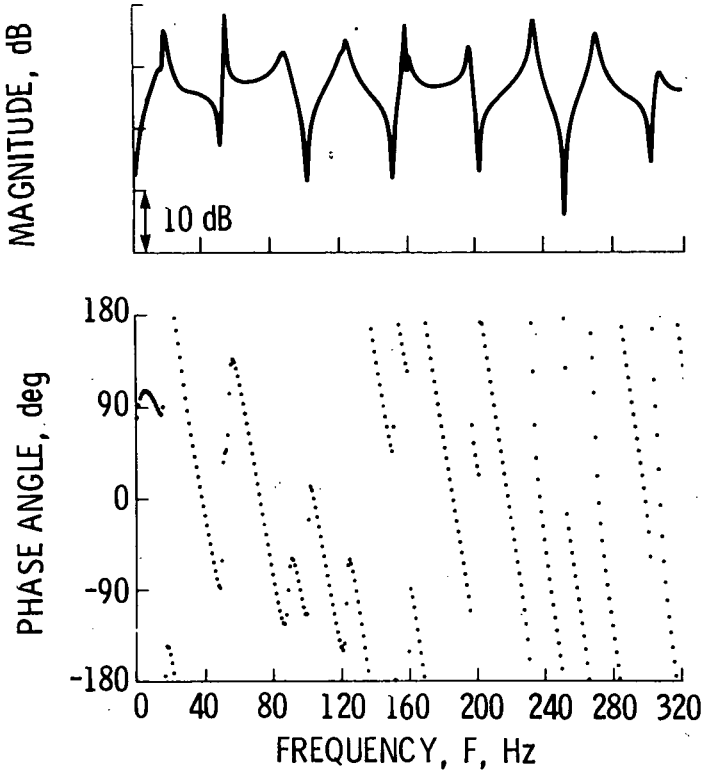

(b) Calculated pressure temperature cross spectrum (t_{CIN} = 288 K, σ = 0.5).

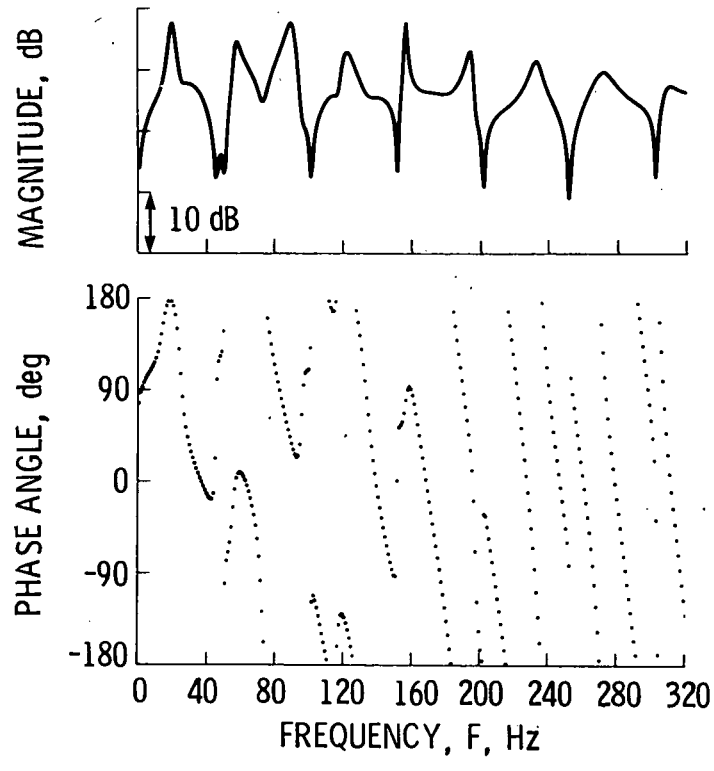

(c) Calculated pressure temperature cross spectrum (t_{CIN} = 288 K, σ = 0.1).

Figure 16. - Concluded.

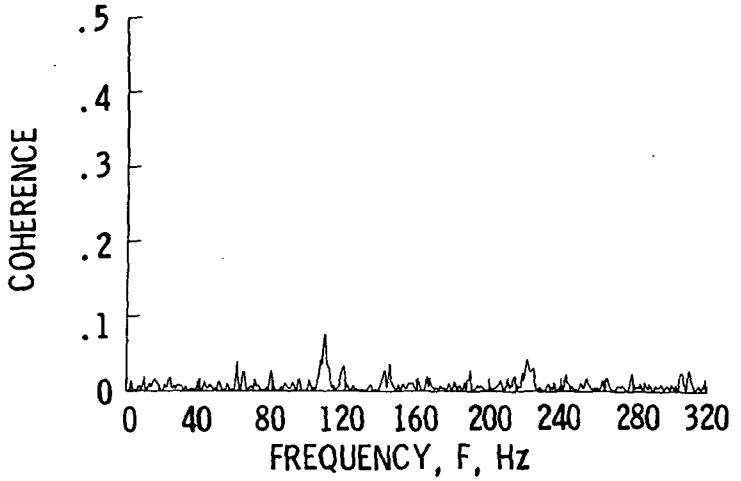

Figure 17. - Coherence between pressure and temperature near duct exit, $|p_4 t_4^*|^2 / |p_4|^2 |t_4|^2$ for test 115 (bandwidth = 0.8 Hz).

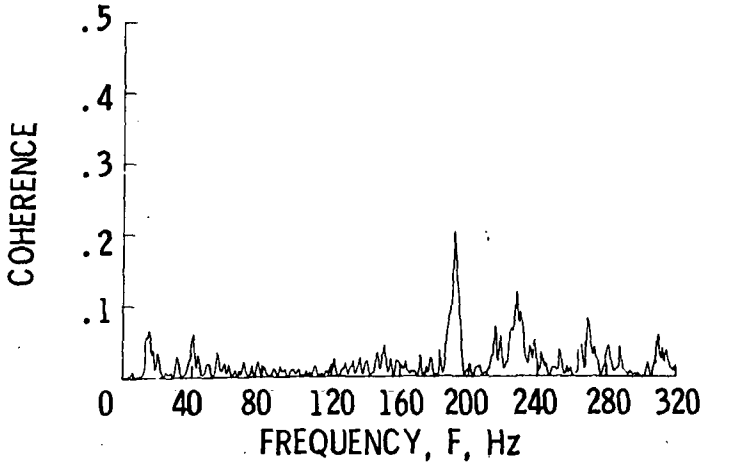

Figure 18. - Coherence between pressure and temperature near duct exit, $|p_4 t_4^*|^2 / |p_4|^2 |t_4|^2$ for test 117 (bandwidth = 0.8 Hz).

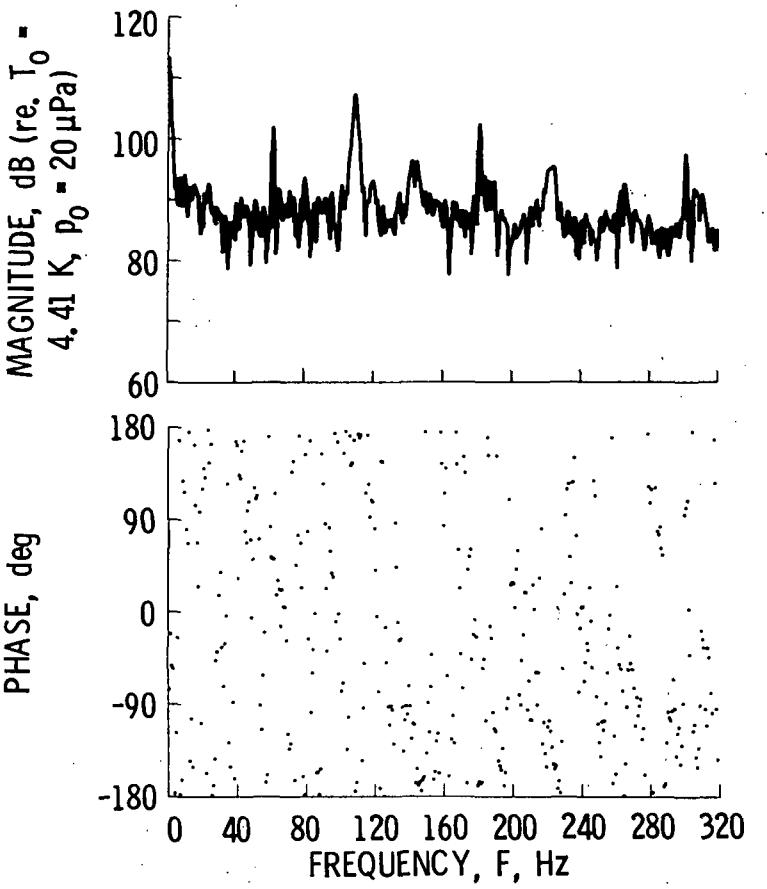

(a) Measured pressure temperature cross spectrum with a bandwidth of 0.8 Hz.

Figure 19. - Pressure temperature cross spectra near duct exit p_4t_4* for test 115.

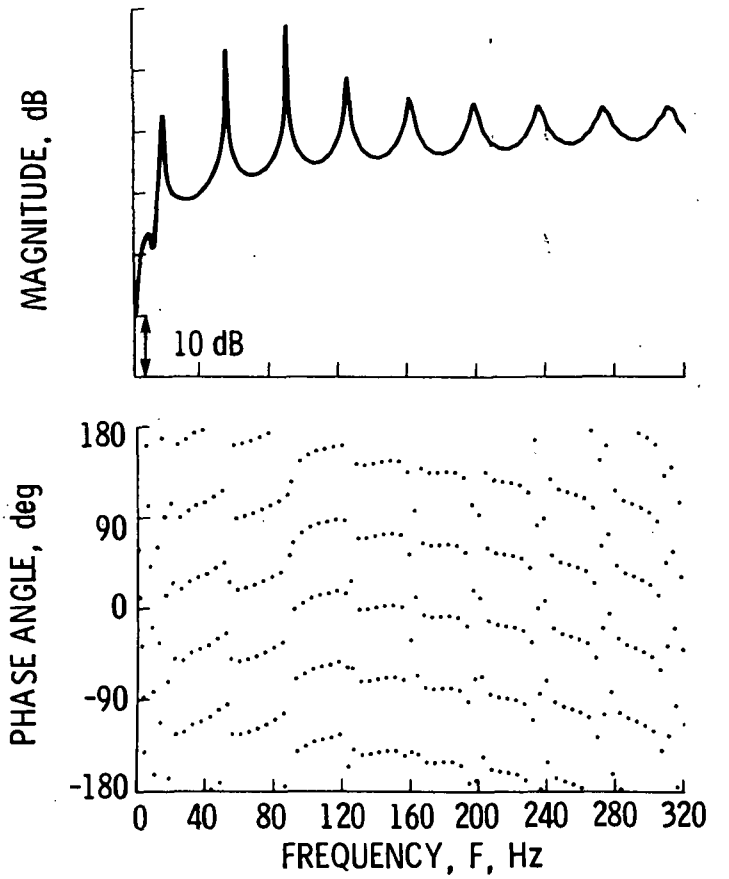

(b) Calculated pressure temperature cross spectrum (t_{CIN} = 288 K, σ = 0.5).

Figure 19. - Continued.

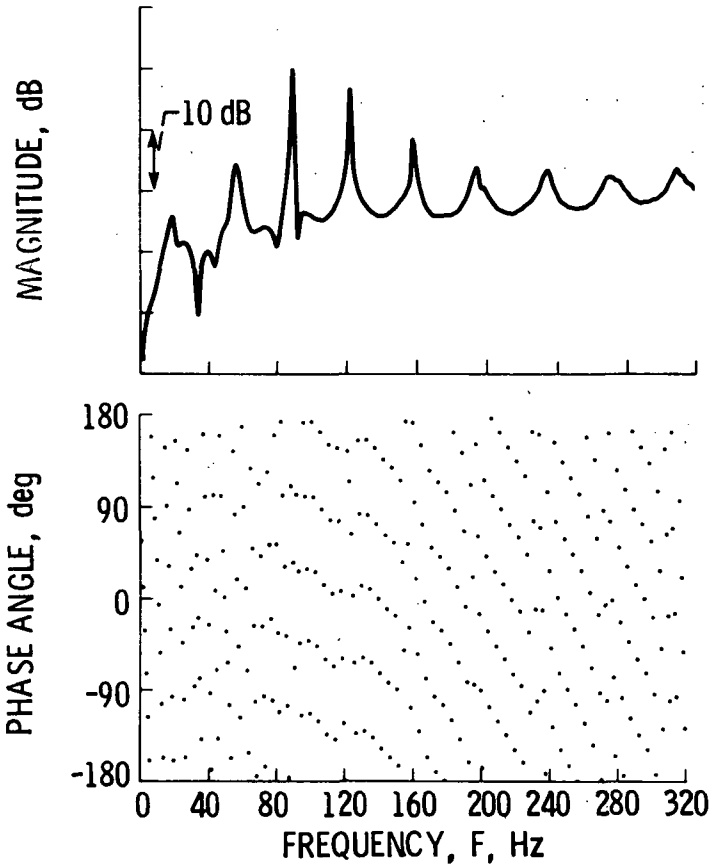

(c) Calculated pressure temperature cross spectrum (T_{CIN} = 288 K, σ = 0.1).

Figure 19. - Concluded.

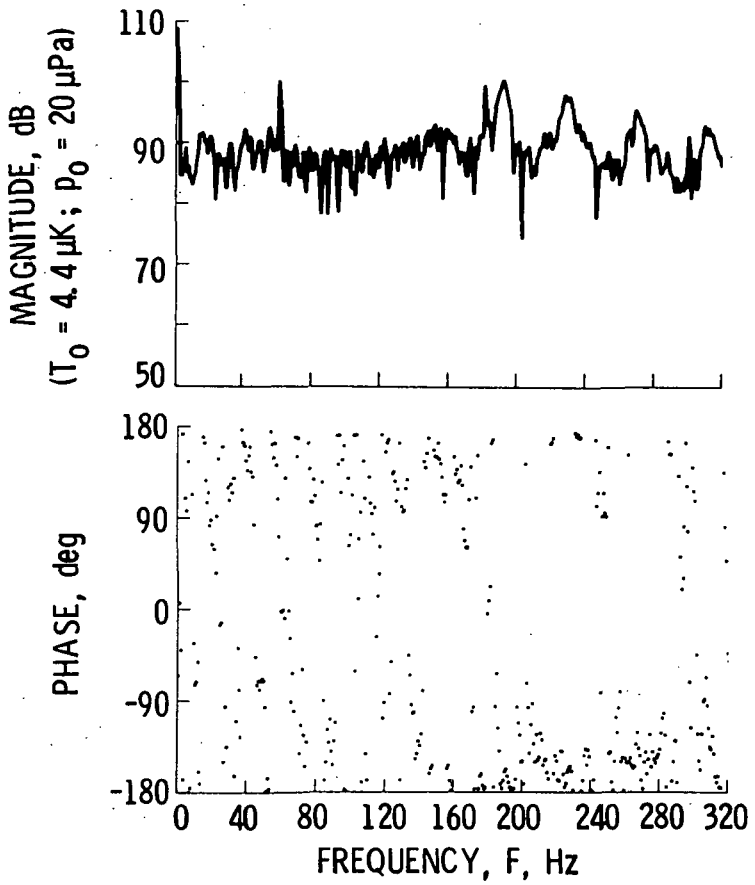

(a) Measured pressure temperature cross spectrum $p_4t_4^*$ for a bandwidth of 0.8 Hz.

Figure 20. - Pressure temperature cross spectra near duct exit $p_4t_4^*$ for test 117.

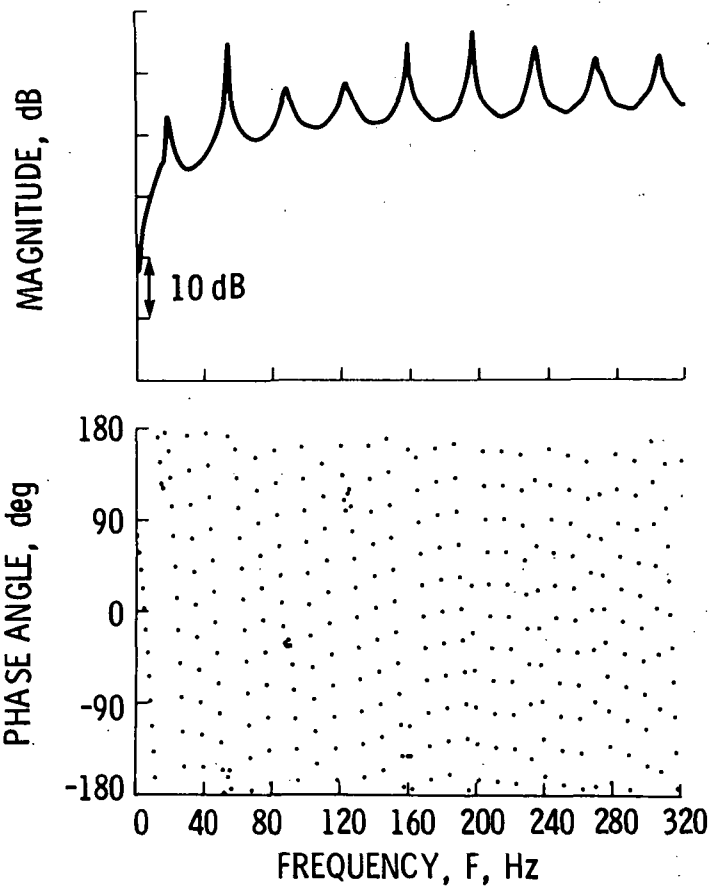

(b) Calculated pressure temperature cross spectrum ($t_{CIN} = 288$, $\sigma = 0.5$).

Figure 20. - Continued.

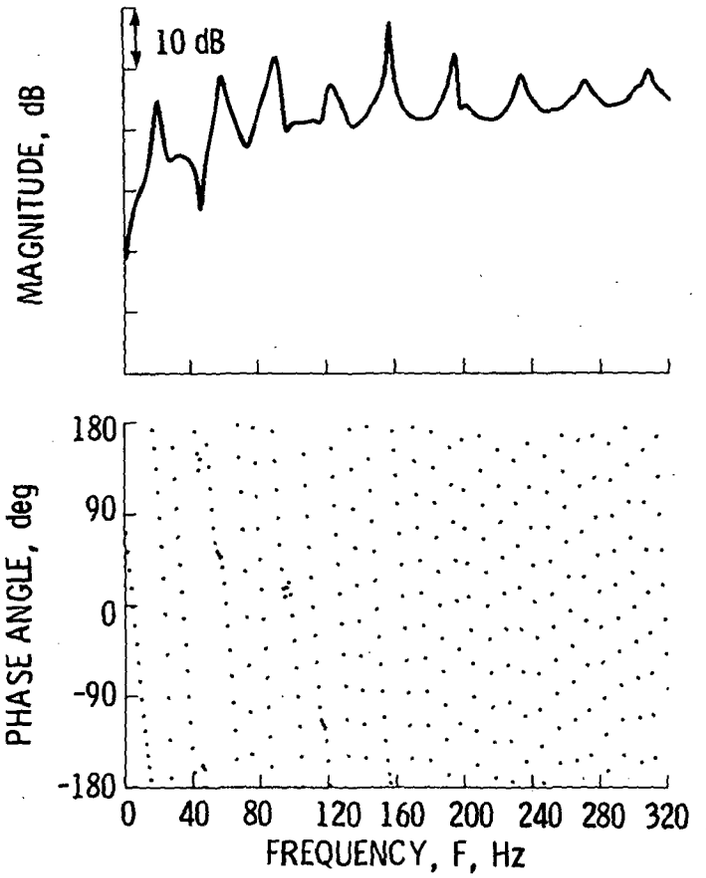

(c) Calculated pressure temperature cross spectrum (t_{CIN} = 288 K, σ = 0.1).

Figure 20. - Concluded.

1. Report No.	2. Government Accession No.	3. Recipient's Catalog No.
NASA TM-83671		

4. Title and Subtitle	5. Report Date
A Theoretical Model for the Cross Spectra Between Pressure and Temperature Downstream of a Combustor	6. Performing Organization Code 505-31-3B
7. Author(s)	8. Performing Organization Report No. E-2114
J. H. Miles and E. A. Krejsa	10. Work Unit No.
9. Performing Organization Name and Address	11. Contract or Grant No.
National Aeronautics and Space Administration Lewis Research Center Cleveland, Ohio 44135	13. Type of Report and Period Covered Technical Memorandum
12. Sponsoring Agency Name and Address	14. Sponsoring Agency Code
National Aeronautics and Space Administration Washington, D.C. 20546	

15. Supplementary Notes

Prepared for the One hundred seventh Meeting of the Acoustical Society of America, Norfolk, Virginia, May 6-10, 1984.

16. Abstract

A theoretical model developed to calculate pressure-temperature cross spectra, pressure spectra, temperature spectra and pressure cross spectra in a ducted combustion system is presented. The model assumes the presence of a fluctuating-volumetric-heat-release-rate disk source and takes into account the spatial distribution of the steady-state volumetric-heat flux. Using the model, pressure, velocity, and temperature perturbation relationships can be obtained. The theoretical results show that, at a given air mass flow rate, the calculated pressure-temperature cross spectra phase angle at the combustor exit depends on the model selected for the steady-state volumetric-heat flux in the combustor. Using measurements of the phase angle, an appropriate source region model was selected. The model calculations are compared with the data. The comparison shows good agreement and indicates that with the use of this model the pressure-temperature cross spectra measurements provide useful information on the physical mechanisms active at the combustion noise source.

17. Key Words (Suggested by Author(s))	18. Distribution Statement
Acoustics; Noise (sound); Aeroacoustics; Propagation; Ducts; Thermocouples; Combustion	Unclassified - unlimited STAR Category 71

19. Security Classif. (of this report)	20. Security Classif. (of this page)	21. No. of pages	22. Price*
Unclassified	Unclassified		

*For sale by the National Technical Information Service, Springfield, Virginia 22161

National Aeronautics and
Space Administration

Washington, D.C.
20546

Official Business
Penalty for Private Use, $300

SPECIAL FOURTH CLASS MAIL
BOOK

Postage and Fees Paid
National Aeronautics and
Space Administration
NASA-451

NASA

POSTMASTER: If Undeliverable (Section 158
Postal Manual) Do Not Return